Science
AAAS

Supplementary Materials for

Engineering longevity—design of a synthetic gene oscillator to slow cellular aging

Zhen Zhou *et al*.

Corresponding author: Nan Hao, nhao@ucsd.edu

Science **380**, 376 (2023)
DOI: 10.1126/science.add7631

The PDF file includes:

Other Supplementary Material for this manuscript includes the following:

Materials and Methods

Strain and plasmid construction

Standard protocols were used for molecular cloning. All yeast strain used in this study were constructed based on BY4741 (*MAT*a *his3*Δ1 *leu2*Δ0 *met15*Δ0 *ura3*Δ0). Details of strains, plasmids, and primers are included in Table S1-S3.

To make the plasmid for replacing the native *SIR2* promoter by P_{CYC1} (NHB1075), Gibson Assembly (NEB) was used with a 451 bp DNA fragment that is 468 bp upstream of the *SIR2* start codon (F1), *URA3* from pRS306 plasmid (F2), a 501 bp DNA fragment that is 410 bp upstream from the *SIR2* start codon (F3), the *CYC1* promoter (F4: 468 bp), a 474 bp fragment of the *SIR2* open reading frame (ORF) starting from the start codon (F5), a fragment from pRS306 containing an autonomously replicating sequence (ARS) and ampicillin resistance gene (F6), to yield the plasmid NHB1075 (Fig. S19A).

To make the plasmid for the single-copy rDNA-GFP reporter (NHB0730), a DNA fragment containing the unique sequence at the left edge of the rDNA region (*52*) and an *XhoI* restriction site at 5' end (F7), a 680 bp fragment of the *TDH3* promoter (F8), a 717 bp *GFP* ORF (F9), a 420 bp DNA fragment that is 196 bp downstream from the left edge of the rDNA region (F10), the *URA3* expression cassette (F11), the F10 fragment with a *BamHI* restriction site (F12), were assembled together with F6 to make the plasmid (NHB0730) (Fig. S19B).

To make the plasmid for integration of P_{TDH3}-*HAP4* or P_{ADH1}-*HAP4* fragment into the non-transcribed spacer 1 (*NTS1*) at the rDNA region, the P_{TDH3}-*GFP* fragment of the rDNA-GFP reporter (NHB0200) (*32*) was replaced by P_{TDH3}-*HAP4* or P_{ADH1}-*HAP4* by Gibson assembly, yielding the plasmid NHB1048 and NHB1333, respectively. The *HindIII* (AAGCTT) restriction site at *HAP4* ORF was synonymously mutated to ATGCTT, so that the plasmid has a unique

HindIII site located within the *NTS1* homologous part of the plasmid for further linearization and integration into the rDNA region in the genome.

The synthetic oscillator strain was constructed by following 5 steps: 1, In the WT strain with nuc. iRFP (NH0263), *mCherry-LEU2* was amplified by PCR and integrated at the C-terminus of *SIR2* by homologous recombination to create the *SIR2-mCherry* strain (NH1378) ; 2, To replace the native *SIR2* promoter with P_{CYC1}, the strain NH1378 was transformed with the DNA fragment F1-F5 amplified by PCR from NHB1075 to replace P_{SIR2} with fragment containing F1-F4, *URA3* was replaced through homologous recombination of F1 and F3, and the strain was selected on 5'-FOA plate to create the P_{CYC1}-*SIR2-mCherry* strain (NH1382) (Fig. S19A); 3, In the strain NH1382, the *HAP4* ORF was replaced by *HIS3* by homologous recombination (NH1391); 4, The strain NH1391 was transformed with the DNA fragment F7-F12 from NHB0730 by *BamHI* and *XhoI* digestion. *URA3* was removed through homologous recombination of F10 and F12 with selection on 5'-FOA to incorporate the single-copy rDNA-GFP reporter (NH1571) (Fig. S19B); 5, The strain NH1571 was transformed with NHB1048 linearized by *HindIII* digestion at the *NTS1* homologous part of the plasmid to insert P_{TDH3}-*HAP4* into the rDNA region, creating the synthetic oscillator strain NH1574.

To make the strain with two copies of *SIR2* (NH1855), NH1545 was transformed with *SphI* digested plasmids from NHB0638; To make the strain of O/E *HAP4* (NH1857), NH1545 was transformed with *BsmI* digested plasmids from NHB0659; To make 2x *SIR2* + O/E *HAP4* strain (NH1802), NH1545 was transformed with *BsmI* digested plasmids from NHB0659 and *SphI* digested plasmids from NHB0299 sequentially.

To make the strain without negative feedback loop, NH1382 was transformed *HindIII* digested plasmid from NHB0730.

To make the strain without feedforward loop, the very basic strain (NH268) was firstly transformed with *BamHI* and *XhoI* double digested plasmid from NHB0730 to make single copy rDNA reporter strain (NH1545); *HAP4* was deleted in NH1545 to make NH1725 and *SIR2* was then tagged with *mCherry* to make NH1851; finally, NH1851 was transformed with with *HindIII* digested plasmid from NHB1048.

To make the strain with weak feedforward loop, NH1571 was transformed with *HindIII* digested plasmid from NHB1333.

To make *fob1*Δ *sch9*Δ double mutants, the *URA3* and *HIS3* fragments were amplified from pRS306 and pRS303, respectively, to replace the *FOB1* and *SCH9* ORFs in WT, respectively, by homologous recombination.

The processes for making other single or double mutants were the same as described above.

All transformations were performed with the standard lithium acetate method, and integration was confirmed by PCR.

Computational modeling

For the synthetic oscillator, the circuit is described as the following delay differential equations (DDEs):

$$\frac{dmS}{dt} = \alpha_{S0} + \alpha_S \frac{H(t-\tau_H)^{n_1}}{K_H^{n_1} + H(t-\tau_H)^{n_1}} - \delta_m \cdot mS \qquad (1)$$

$$\frac{dmH}{dt} = \alpha_{H0} + \alpha_H \frac{K_S^{n_2}}{K_S^{n_2} + S(t-\tau_S)^{n_2}} - \delta_m \cdot mH \qquad (2)$$

$$\frac{dS}{dt} = \beta \cdot mS - \delta_S \cdot S \qquad (3)$$

$$\frac{dH}{dt} = \beta \cdot mH - \delta_H \cdot H \qquad (4)$$

where mS, mH, S and H are the levels of *SIR2* mRNA, HAP mRNA, Sir2 protein and HAP protein, respectively. τ_S and τ_H are time delays for Sir2 protein and HAP protein, respectively.

For plotting the phase plane in Fig. 1B, we used the same deterministic model for the Sir2-HAP toggle switch circuit, as described previously (*34*). For plotting the phase plane in Fig. 1C, the synthetic oscillator circuit is described by two delay differential equations from the semi-stable equilibrium of equation (1) and (2). Basically, assuming mRNA transcription is a fast process, so that both $\frac{dmS}{dt}$ and $\frac{dmH}{dt}$ equal 0.

then (1) and (2) become:

$$mS = \frac{\alpha_{S0}}{\delta_m} + \frac{\alpha_S}{\delta_m} \cdot \frac{H(t-\tau_H)^{n_1}}{K_H{}^{n_1} + H(t-\tau_H)^{n_1}} \tag{5}$$

$$mH = \frac{\alpha_{H0}}{\delta_m} + \frac{\alpha_H}{\delta_m} \cdot \frac{K_S{}^{n_2}}{K_S{}^{n_2} + S(t-\tau_S)^{n_2}} \tag{6}$$

Respectively, plugging (5) and (6) into (3) and (4), we have:

$$\frac{dS(t)}{dt} = \beta\frac{\alpha_{S0}}{\delta_m} + \beta\frac{\alpha_S}{\delta_m} \cdot \frac{H(t-\tau_H)^{n_1}}{K_H{}^{n_1} + H(t-\tau_H)^{n_1}} - \delta_S \cdot S(t) \tag{7}$$

$$\frac{dH(t)}{dt} = \beta\frac{\alpha_{H0}}{\delta_m} + \beta\frac{\alpha_H}{\delta_m} \cdot \frac{K_S{}^{n_2}}{K_S{}^{n_2} + S(t-\tau_S)^{n_2}} - \delta_H \cdot H(t) \tag{8}$$

Parameters, except two new parameters τ_H and τ_S, were used with the same values as those used in the ordinary differential equations (ODEs) in Fig. S2 to generate oscillations (Table S4).

The Monte Carlo method for parameter exploration

The physiological ranges of parameter values for the ODE model of the synthetic oscillator (Fig. S2B) were roughly estimated based on the information of gene expression and protein

concentrations from SGD (https://www.yeastgenome.org/). One million different sets of parameter values were randomly generated within physiological parameter ranges and were tested for oscillation generation. For oscillation identification, we used the method described previously in Pušnik's work (*53*). Specifically, to eliminate the possibility of damped oscillation, we took only the last 50% of the time trace from each simulation into consideration. Fast Fourier Transformation (FFT) was used to transfer the signal to the frequency domain, in which the indexes of peaks (P_i) were recorded. The oscillation occurs, if the cost function of the vector of parameters meets such criteria:

$$C(\theta) = -\max\{\frac{\sigma(A_{p_{i-\gamma}} \cdots A_{p_{i+\gamma}})}{A_{P_i}}\} < C_0,$$

where A_{P_i} is the amplitude of the transformed signal in the frequency domain at frequency P_i of the i-th peak, σ is standard deviation for the i-th peak in the neighboring window of size 1 (γ=1), θ is the vector of candidate parameters, C_0 is the threshold for categorizing candidates as oscillation or not. Since a large pulse could also generate a "fat" peak in the frequency domain, we used a narrow window to promote sharp peaks, avoiding such a scenario. For each parameter, all parameter values that gave rise to oscillation were recorded and showed in the red boxplots in Fig. S3A, whereas the values that failed to generate oscillation were shown in the blue boxplots. About 0.3% of the 1 million parameter sets tested generated oscillations.

Bifurcation diagram

To investigate the dependence of oscillation on the parameters identified using the Monte Carlo method, we performed bifurcation analysis with MatCont (*54*). We used the parameter

values listed in Table S4 and changed the values of parameters of interest with other parameters fixed (Fig. S3B).

Setting up microfluidic experiments

The microfluidic devices and experimental setup were described previously (*32, 34, 47, 55, 56*). Yeast cells were inoculated into 2 ml of synthetic complete medium (SD, 2% glucose) and cultured overnight at 30℃. From this culture, 2µl of the saturated culture was diluted into 20 ml of fresh SD medium until its OD_{600} reached ~ 0.9. The chip containing four microfluidic devices was placed under vacuum for 20 min. Meanwhile, 50 ml of SD medium with 0.04% Tween-20 (Sigma) was filled into a 60 ml syringe (Luer-Lok Tip, BD) to which plastic tubing (TYGON, ID 0.020 IN, OD0.060 IN, wall 0.020 IN) was connected. After vacuum, the device was quickly connected to the prepared syringe through plastic tubing from its inlet port. The outlet of the microfluidic device was also connected to plastic tubing. The chip with inlet and outlet connected was then fixed onto the motorized stage of the microscope ready for cell loading. For cell loading, cells were transferred into a 60 ml syringe with plastic tubing connected. The media supply tubing into the inlet was then replaced with the tubing connected to the cell loading syringe. The flow of medium in the device was maintained by gravity to drive cells into traps. After loading, the media supply syringe and tubing were switched back to the inlet of the device. Heights of all tubing were adjusted to make the height difference around 240 cm. Tween-20 is a non-ionic surfactant that helps reduce cell friction on the PDMS of the chip. We have validated previously that this low concentration of Tween-20 has no significant effect on cellular lifespan or physiology (*32*).

Time-lapse microscopy

Time-lapse microscopy experiments were conducted using a Nikon Ti-E inverted fluorescence microscope with an EMCCD camera (Andor iXon X3 DU897). The light source is a spectra X LED system. Images were taken using a CFI plan Apochromat Lambda DM 60X oil immersion objective (NA 1.40 WD 0.13MM). In all experiments, the images were acquired for each fluorescence channel every 15 min for a total of 90 to 110 hours. The exposure and intensity setting for each channel were set as follows: Phase 50 ms, GFP 3 ms at 10% lamp intensity with an EM Gain of 50, mCherry 90 ms at 10% lamp intensity with an EM Gain of 200, and iRFP 300 ms at 15% lamp intensity with an EM Gain of 300.

Quantification of single-cell aging traces

Image processing was conducted using a custom MATLAB code (*32, 34*). The background of images from each fluorescence channel were subtracted. Cell nuclei were masked by thresholding iRFP or Sir2-mCherry signal. The mean intensity value of the top 40% of the pixels of fluorescence reporters was quantified, as described previously (*32, 34*). The time traces of reporters were smoothed using MATLAB function *smoothdata* with specification of the Gaussian method through a 15-element sliding window (Fig. S6A).

To plot the cell cycle length changes as a function of the percentage of lifetime, the vector of cell cycle length was interpolated to a new vector of 100 elements at evenly distributed 100 query points. For single cell aging dynamics and replicative lifespan (RLS) analyses, we collected data from at least 3 independent experiments. Any cells showing obvious abnormal morphologies upon cell loading were filtered out for RLS analysis. Any cells showing dislocation of reporter mask were filtered out for time trace analysis but included in RLS analysis. Significant numbers

for RLS changes were calculated with Gehan-Breslow-Wilcoxon test by using Prism GraphPad 7 (GraphPad Software, CA).

Quantification of the amplitude and period of Sir2 oscillatory pulses

Peaks (P_i) and valleys (V_i) of oscillations of Sir2 trajectories for each single cell were identified by iPeak (from MathWorks File Exchange), where *i* denotes the *i*-th peak or valley. The baseline was formed by connecting all valleys with the polyline (Fig. S6B, black dashed line). The amplitude (A_i) was measured as the vertical distance from P_i to the baseline between V_{i-1} and V_i (Fig. S6B). To define the peaks of oscillation, only the peaks with an amplitude at least five times higher than the average amplitude of fluctuation pulses in WT cells were considered as the "oscillatory pulses" that came from the synthetic oscillation circuit (Fig. S6, B and C). The period (T_i) for each oscillatory pulse was measured as the time span between valley V_{i-1} and V_i (Fig. S6, B and C).

Spectral analysis of Sir2 oscillations

Time traces of Sir2-mCherry were detrended (with Matlab function "detrend(x,n), n=2") from raw data without smoothing and then Fast Fourier transformed (FFT) and squared (Fig. S7A). The power spectrum of an individual time trace was calculated as $P(f) = \frac{|FFT(D(t))|^2}{N}$. Based on the periods of single pulses of oscillator and WT cells (ranging from 1.2 h to 23 h), time traces shorter than 23 hours or deviated before 23 hours were not applied to FFT. To plot average power spectrum for all cells, $P(f)$ of each cell was firstly linear interpolated at 5000 query frequency points which were uniformly distributed along the frequency range. Average power $<\boldsymbol{P}(f_i)>$ was then calculated at each query frequency point f_i.

Stability determination for Sir2 oscillations

In the synthetic oscillator strain, a fraction of cells showed a deviation from Sir2 oscillation with an abrupt increase of Sir2 level late in their lifespan (Fig. S5). To quantitatively determine the stability of Sir2 oscillation for each single cell, we applied the changepoints detection method described in previous studies (*57, 58*). The changepoints were calculated with MATLAB *findchangept* function. In brief, we assumed the time trace of Sir2 ($s_{0:w}$) has a set of K change points $T_w=\{t:0=t_0<\cdots<t_{K-1}<t_K=w\}$, then the function minimizes.

$$F(K)=\sum_{r=0}^{K-1}\sum_{i=t_r}^{t_{r+1}-1}\Delta(s_i;S([s_{t_r}\cdots s_{t_{r+1}-1}]))+\beta K$$

where β is the fixed penalty added for each changepoint, and S is the time trace of Sir2 within s_{t_r} and $s_{t_{r+1}-1}$. Δ is the deviation measurement following the cost function:

$$\sum_{i=t_r}^{t_{r+1}-1}\Delta(s_i;S([s_{t_r}\cdots s_{t_{r+1}-1}]))=(s_{t_{r+1}-1}-s_{t_r}+1)\ln\sum_{i=t_r}^{t_{r+1}-1}\sigma^2(s_{t_r}\cdots s_{t_{r+1}-1})$$

Here, σ^2 denotes the variance. Cells with a lifetime shorter than 2500 min have 1 changepoint, whereas cells with a lifetime longer than 2500 min could have 2 or more changepoints. For each cell, the Sir2 time trace was therefore divided into 2 or more sections by the changepoint(s) where the standard deviation of the trajectory changed the most (Fig. S8). The mean of each section was calculated (m_i). The ratio for the mean value of the last section divided by that of the next to last section ($\frac{m_{end}}{m_{end-1}}$) was defined as the changing ratio for the Sir2 trace. The cells with changing ratios larger than 1 (n=91 out 113) were sorted based on their changing ratios in an increased order. The changepoints detection method was applied to the resulting changing ratio trajectory across cells to identify the turning point on the trajectory, which serves as the threshold (THR; horizontal red

dash line in Fig. S8A) for sustained oscillations vs deviations. The cells with changing ratios above the threshold were considered deviations from the oscillation.

Quantification of the continuous times at the rDNA silencing loss or heme depletion state

The threshold (red dash line in Fig. S14A) for the state of rDNA silencing loss was defined as the third quartile (75th percentile) of all the rDNA-GFP fluorescence values measured from WT and synthetic oscillator strain. The portions of time traces above the threshold represent the state of silencing loss (red portions in Fig. S14A). The mean value of the continuous time spans at this state was calculated for each single aging cell. The threshold (blue dash line in Fig. S14B) for the state of heme depletion was defined as the first quartile (25th percentile) of all the nuc. iRFP fluorescence values measured from the WT and synthetic oscillator strains. The portions of time traces below the threshold represent the state of heme depletion (blue portions in Fig. S14B). The mean value of the continuous time spans at this state was calculated for each single aging cell. Continuous times at the silencing loss state and the heme depletion state were shown for each single aging cell in Fig. 4C. Continuous durations as a percentage of the cell's lifetime were also calculated to facilitate the comparison among strains with different lifetimes (Figs. S15, S16, and S18).

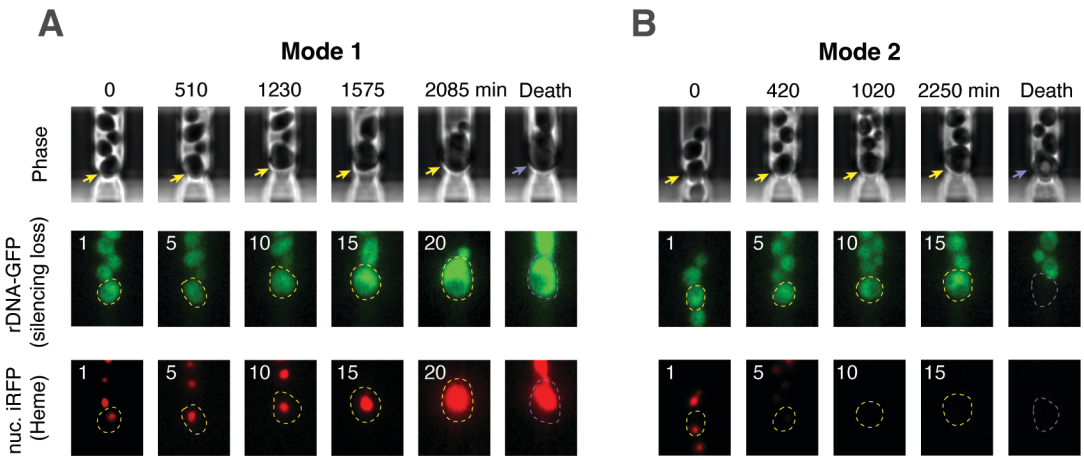

Fig. S1. Representative time-lapse images of WT cells with divergent aging processes. (A) Time-lapse images of a mother cell aging with rDNA silencing loss, previously designated as "mode 1" aging (*34*). (B) Time-lapse images of a mother cell aging with heme depletion, previously designated as "mode 2" aging (*34*). Mode 1 and Mode 2 cells were classified based on their age-dependent changes in their daughter morphologies (Mode 1 – elongated daughters; Mode 2 – smaller round daughters) and dynamics of iRFP fluorescence (*34, 55*). Time-lapse images are shown for (top) Phase, (middle) rDNA-GFP, and (bottom) nuc. iRFP of the same cells. Replicative age of the mother cell is shown at the top left corner of each image. For phase images, aging and dead mother cells are marked by yellow and purple arrows, respectively. In fluorescence images, aging and dead mother cells are circled in yellow and purple, respectively.

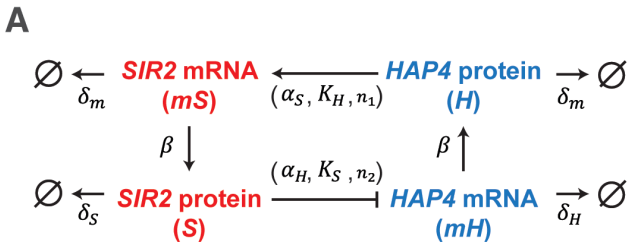

$$\frac{dmS}{dt} = \alpha_{S0} + \alpha_S \frac{H^{n_1}}{K_H{}^{n_1} + H^{n_1}} - \delta_m \cdot mS$$

$$\frac{dmH}{dt} = \alpha_{H0} + \alpha_H \frac{K_S{}^{n_2}}{K_S{}^{n_2} + S^{n_2}} - \delta_m \cdot mH$$

$$\frac{dS}{dt} = \beta \cdot mS - \delta_S \cdot S$$

$$\frac{dH}{dt} = \beta \cdot mH - \delta_H \cdot H$$

Fig. S2. A mathematical model of the gene oscillator circuit. (A) Diagram of the gene oscillator model with a synthetic negative feedback loop. (B) Ordinary differential equations of the gene oscillator model. (C) Example of sustained oscillations in Sir2 and HAP from model simulation (see Materials and Methods for details).

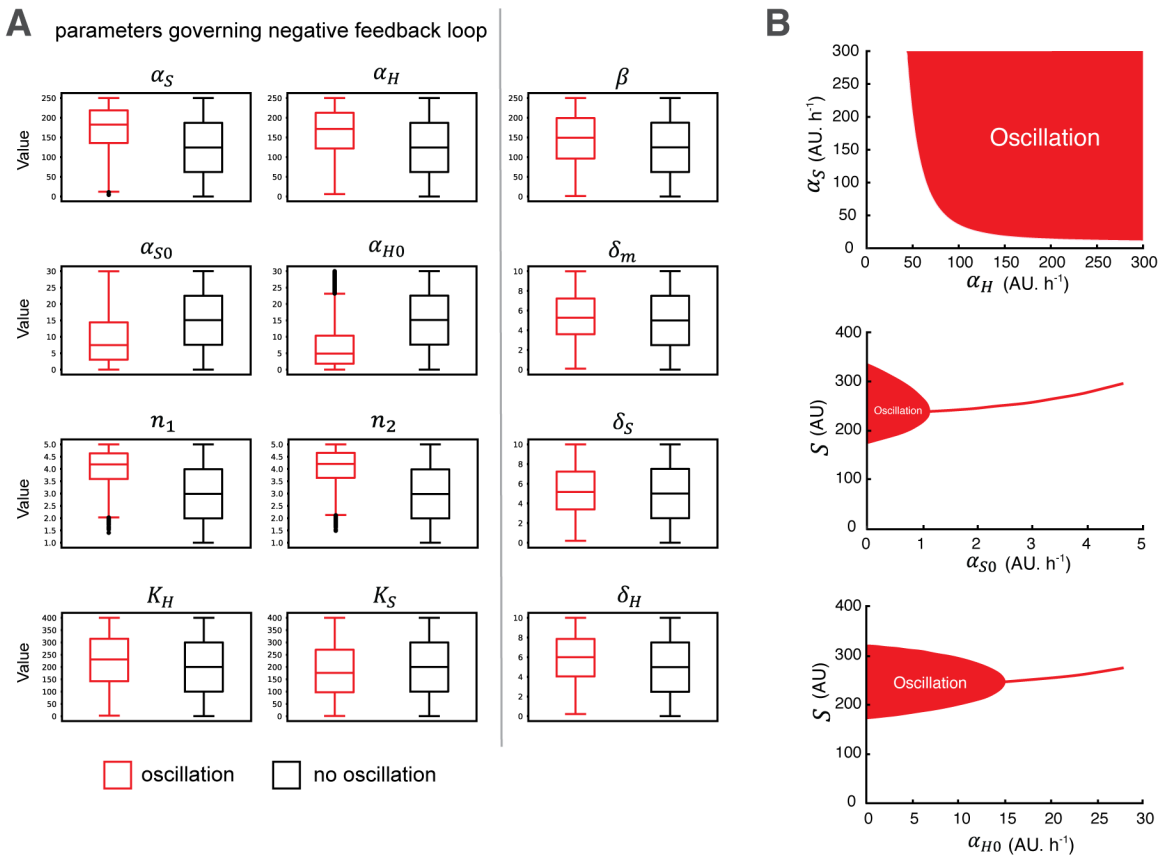

Fig. S3. Exploration of the parameter regime that favors oscillation. (A) Boxplots show the ranges of parameter values that generate oscillation (red) vs no oscillation (black). The Monte Carlo method was used to explore parameter regimes for the model from Fig. S2. Specifically, 1 million different sets of parameter values were randomly generated and were categorized into two groups - the ones that generate sustained oscillation and the ones that cannot generate sustained oscillation (see Materials and Methods for details). For each parameter, the red boxplot shows the range of parameter values from the parameter group that generate oscillations and the black boxplot shows the range of parameter values from the group that cannot generate oscillations. The left two columns show the parameters that govern the synthetic negative feedback loop. The right column shows the parameters that govern mRNA/protein production and degradation. (B) Bifurcation plots show the dependence of oscillations on key parameters identified from the Monte Carlo method. Top: the plot shows how oscillations depend on the strength of *SIR2* induction by HAP (a_S) and the capacity of HAP transcription (a_H). Middle: the plot shows the how oscillations depend on the basal expression of *SIR2* (a_{S0}). Bottom: the plot shows how oscillations depend on the basal expression of HAP upon full Sir2-mediated repression (leakiness from Sir2-mediated transcriptional repression of HAP) (a_{H0}).

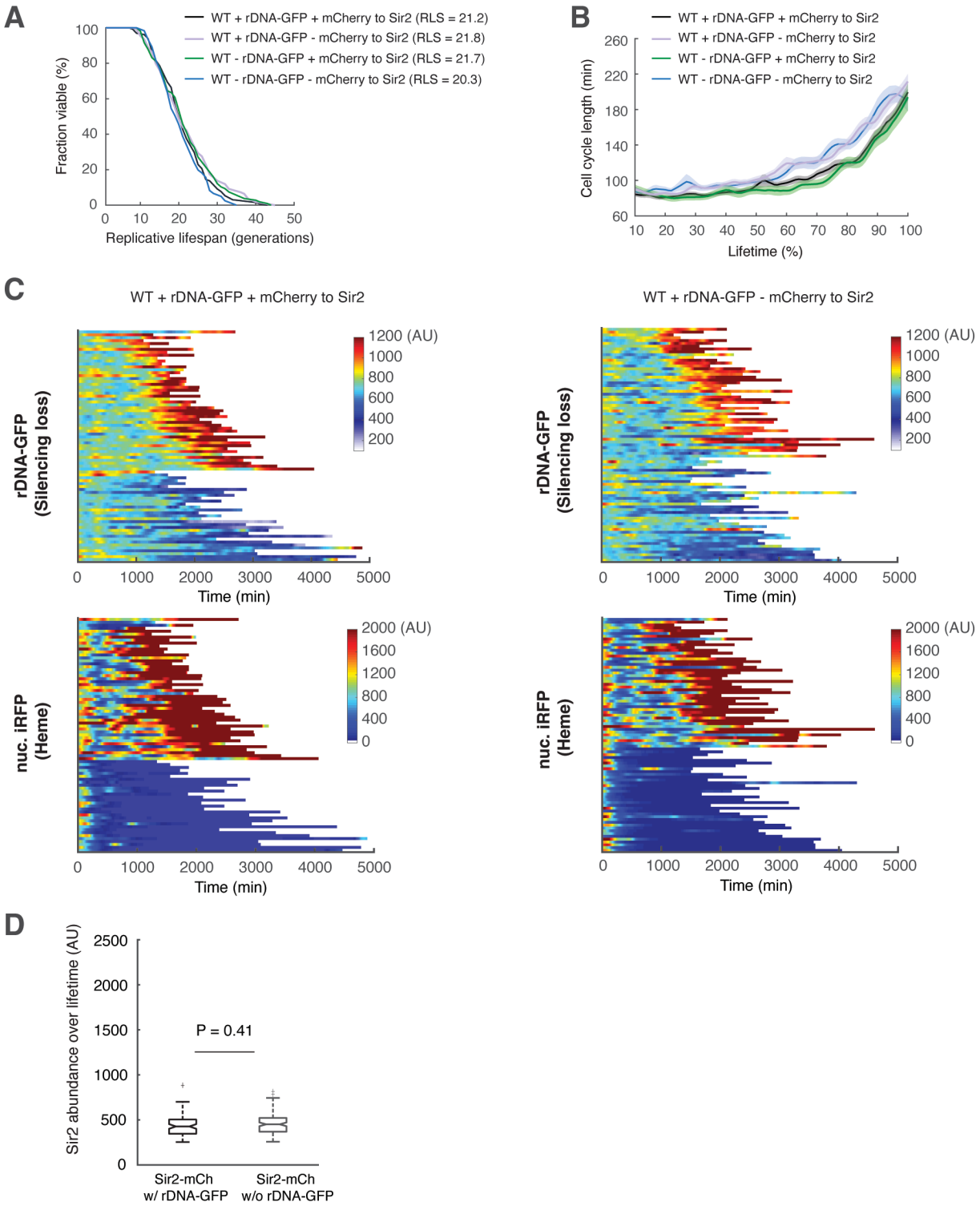

Fig. S4. Effects of the mCherry tag to Sir2 and the rDNA-GFP reporter on yeast aging and growth. (A) Replicative lifespans for WT with (+) rDNA-GFP and with (+) mCherry tag to Sir2 (n=131), WT with (+) rDNA-GFP and without (-) mCherry tag to Sir2 (n=109), WT without (-) rDNA-GFP and with (+) mCherry tag to Sir2 (n=107), and WT without (-) rDNA-GFP and without (-) mCherry tag to Sir2 (n=121). (B) Age-dependent changes of cell cycle length for WT with (+)

rDNA-GFP and with (+) mCherry tag to Sir2, WT with (+) rDNA-GFP and without (-) mCherry tag to Sir2, WT without (-) rDNA-GFP and with (+) mCherry tag to Sir2, and WT without (-) rDNA-GFP and without (-) mCherry tag to Sir2. (C) Single-cell color map trajectories of rDNA-GFP (top) and nuclear-anchored iRFP (bottom) for WT with (+) rDNA-GFP and with (+) mCherry tag to Sir2 and WT with (+) rDNA-GFP and without (-) mCherry tag to Sir2. Each row represents the time trace of a single cell throughout its lifespan. Color represents the fluorescence intensity as indicated in the color bar. (D) Boxplots show the distributions of Sir2 abundance averaged over the lifetimes of single aging cells in WT with Sir2-mCherry, (left) with or (right) without rDNA-GFP. The difference is not significant with $p = 0.41$ in unpaired t-test.

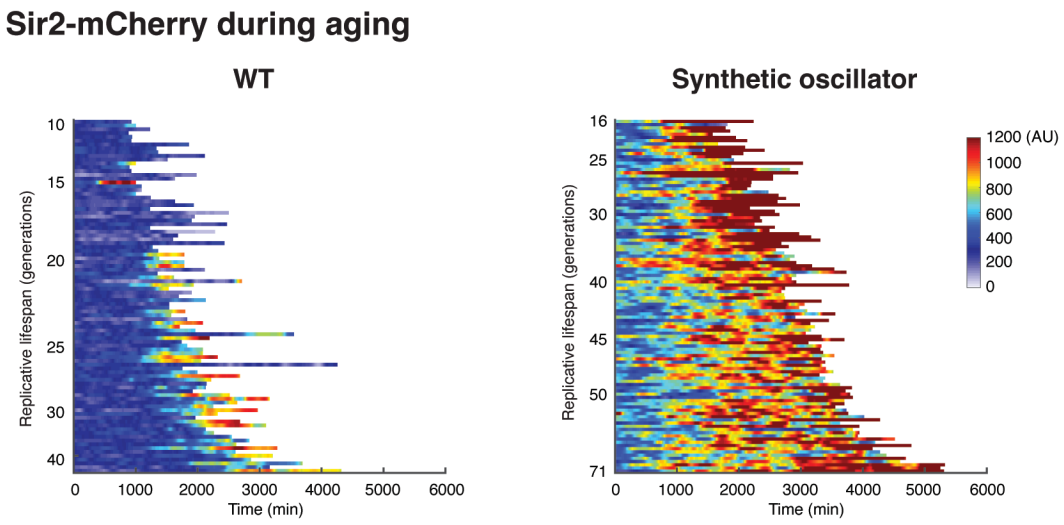

Fig. S5. Color map aging trajectories of Sir2-mCherry for WT (n=93) and the synthetic strain (n=113). Each row represents the time trace of a single cell throughout its lifespan. Color represents the fluorescence intensity as indicated in the color bar. Cells are sorted based on their replicative lifespan (RLS).

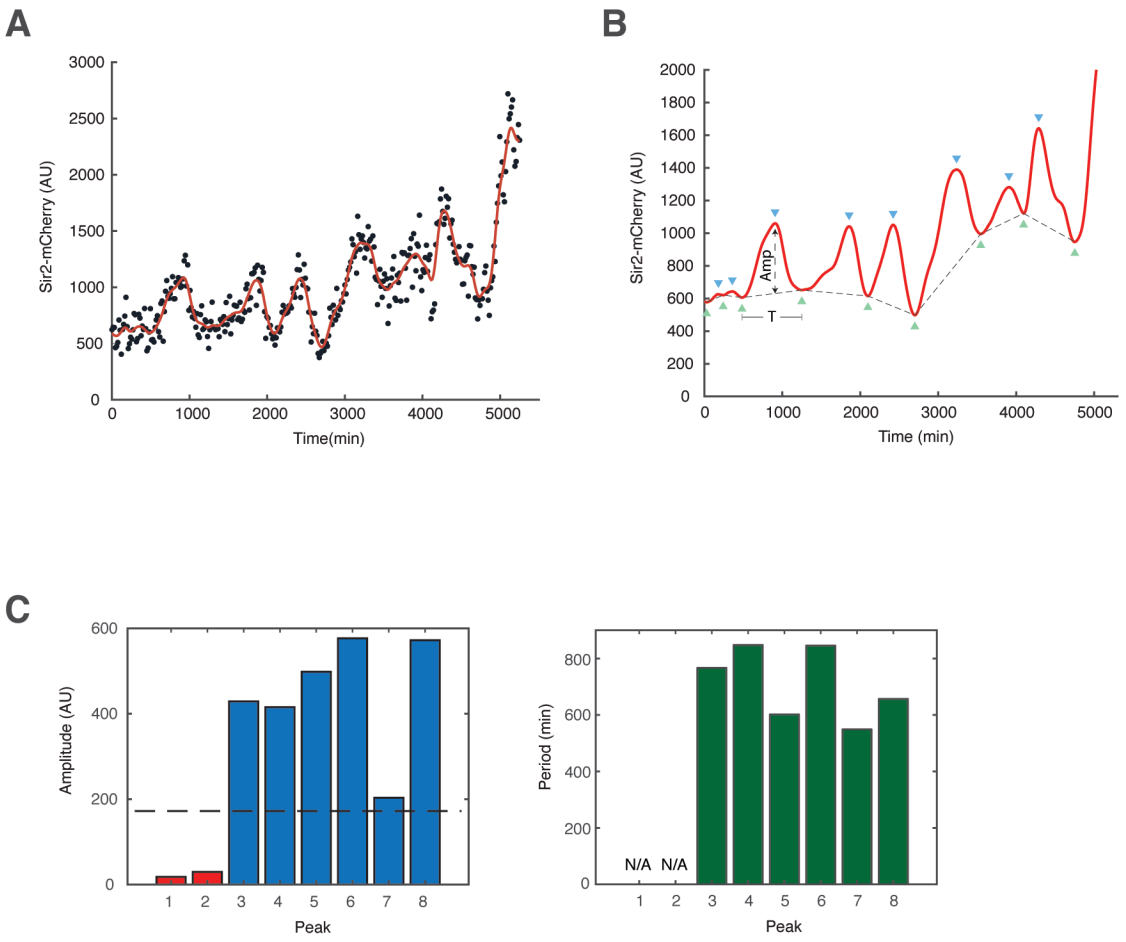

Fig. S6. Quantification of the amplitudes and periods of Sir2 oscillatory pulses. (A) Raw time trace data of Sir2-mCherry in a representative cell to illustrate the process of trace smoothing. Black dots are raw data; red curve is the smoothed time trace. The details of the smoothing method and parameters are provided in Materials and Methods. (B) Illustration for the quantification of the amplitude and period of oscillatory pulses using the representative time trace from (A). Peaks (downward blue triangle) and valleys (upward green triangle) were determined using iPeak (from MathWorks File Exchange). Dashed line represents the baseline which connects all valleys. The amplitude (Amp) of a pulse was calculated as the distance from the peak to the point crossed by the vertical line from the peak to the baseline. The period (T) of a pulse was calculated as the time span between two valleys. (C) Left: Bar graph shows the amplitudes of each pulse in the time trace in (B). Only the pulses with amplitudes over the threshold (dash line - 5 times of the average amplitude of fluctuation pulses in WT) were considered as true oscillatory pulses, as opposed to small fluctuations (Materials and Methods). Right: Bar graph shows the periods of each pulse in the time trace in (B).

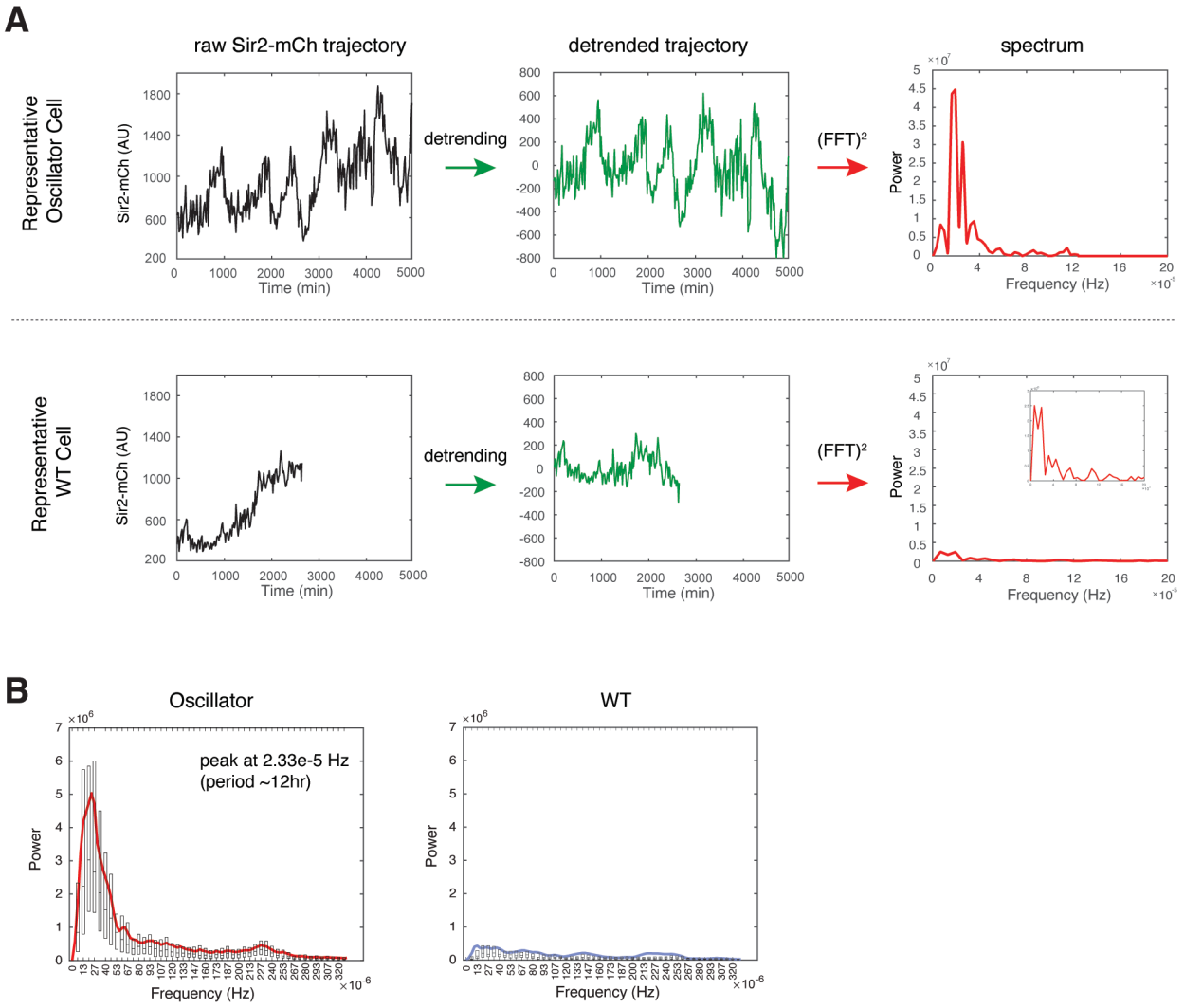

Fig. S7. Spectral analysis of Sir2 oscillations. (A) Illustration of the power spectral computation using single-cell time traces of (top) a representative oscillator cell and (bottom) a WT cell as examples. The time trace of Sir2-mCherry fluorescence was detrended from raw data (no data smoothing) then Fast Fourier transformed (FFT) and squared. The same parameters were used for both the synthetic oscillator strain and WT. Details for the computation pipeline are provided in Materials and Methods. (B) Average power spectrum for (left) the oscillator strain and (right) WT. Boxplots show the frequency-dependent distributions of power spectrum. The bottom and top of the box are first and third quartiles, respectively. The band inside is the median. Average power spectrum of the oscillator strain and WT are shown in red and blue, respectively.

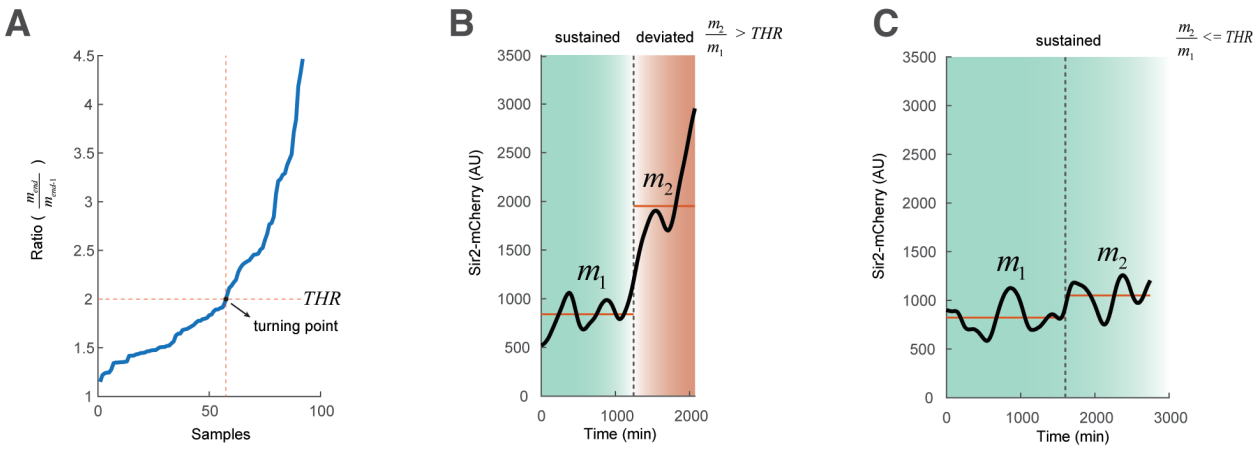

Fig. S8. Stability determination for Sir2 oscillations. (A) Defining the threshold for deviation from oscillations. The changepoints detection method (see Materials and Methods for details) was performed and the changing ratio (m_{end}/m_{end-1}) was calculated for the cells with for the Sir2-mCherry time trace of each single aging cell from the oscillator strain. The cells with changing ratios larger than 1 were then sorted based on their changing ratios (n=91 out of 113). The changepoints detection method was applied to the resulting changing ratio trajectory across cells to identify the turning point on the trajectory, which serves as the threshold (*THR*; horizontal red dash line) for sustained oscillations vs deviations. (B) A representative Sir2-mCherry time trace illustrating the deviation from sustained oscillation with the changing ratio larger than *THR*. The time trace was separated by the change point into sustained region (green) and deviated region (red). (C) A representative Sir2-mCherry time trace illustrating sustained oscillation with the changing ratio smaller than *THR*.

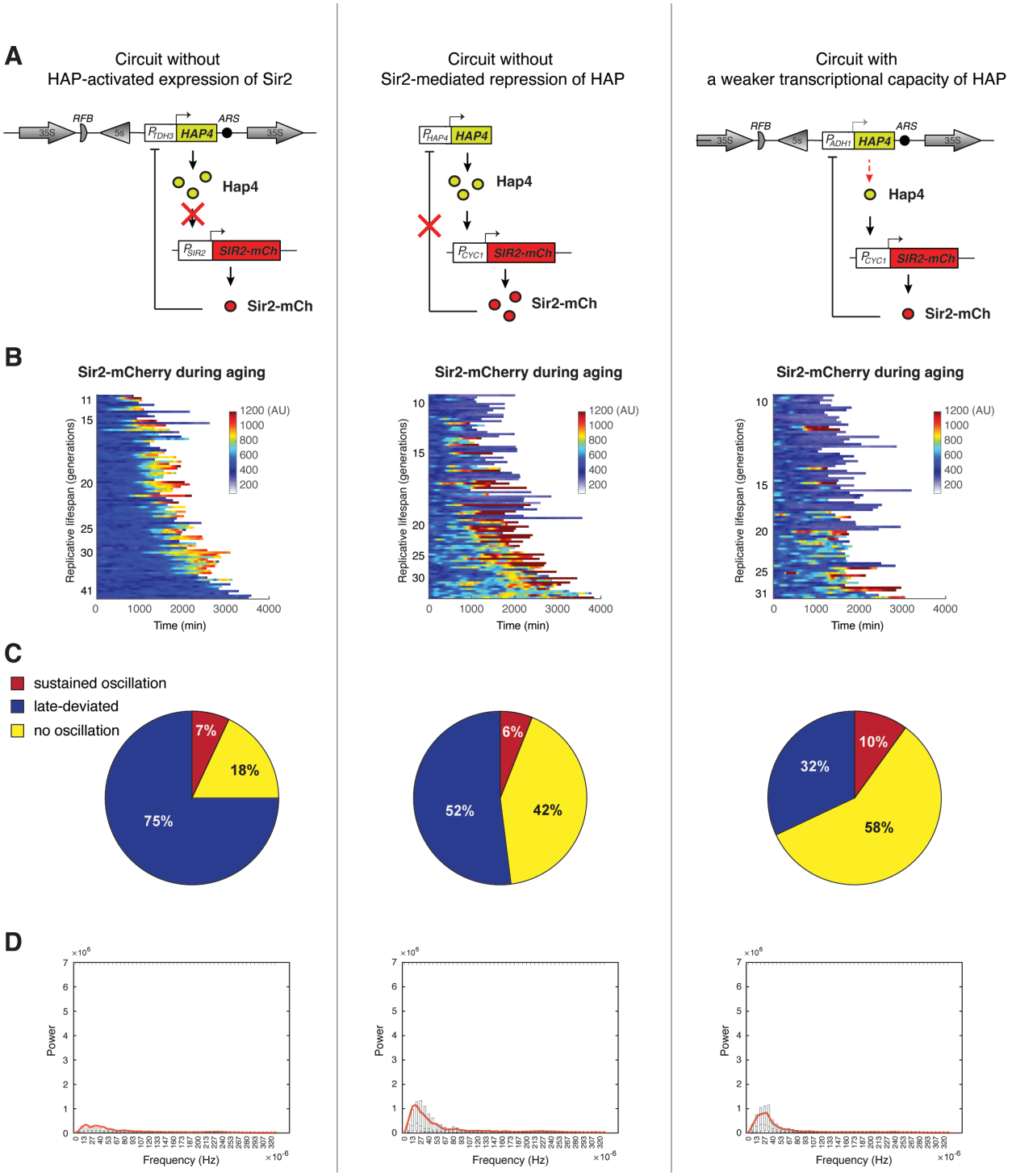

Fig. S9. Synthetic Sir2-HAP circuits with broken or weakened feedback interactions. (A) Diagrams illustrate gene interactions in different versions of the Sir2-HAP circuit. Circuit without HAP-activated expression of Sir2 - *SIR2* is expressed under its native promoter and hence is not regulated by HAP. Circuit without Sir2-mediated repression of HAP – *HAP4* is expressed under its native promoter and is not inserted at rDNA-NTS. Circuit with a weaker transcriptional capacity of HAP – *HAP4* is expressed under the *ADH1* promoter, weaker than the oscillator's *TDH3*

promoter. (B) Color map aging trajectories of Sir2-mCherry for the strains carrying the synthetic Sir2-HAP circuit without HAP-activated expression of Sir2 (n=110), without Sir2-mediated repression of HAP (n=103), or with a weaker transcriptional capacity of HAP (n=84). (C) Proportions of aging cells with different versions of the synthetic circuit that show sustained oscillation or a deviation from oscillation late in life (late-deviated), or no oscillation. (D) Power spectral analysis for aging cells with different versions of the synthetic circuit. For (C) and (D), single-cell data from different strains have been processed through the same analytical pipeline used for the oscillator strain in Fig. 2D and Fig. S7.

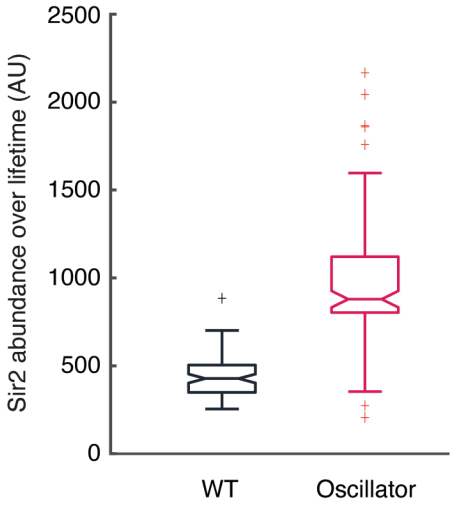

Fig. S10. Sir2 abundance in WT and the oscillator strain. Boxplots show the distributions of Sir2 abundance averaged over the lifetimes of single aging cells in WT (black) and synthetic oscillator strain (red). The mean Sir2 expression level in WT is 439.7 ± 117.6 AU. The mean Sir2 expression level in the oscillator strain is 950 ± 284 AU.

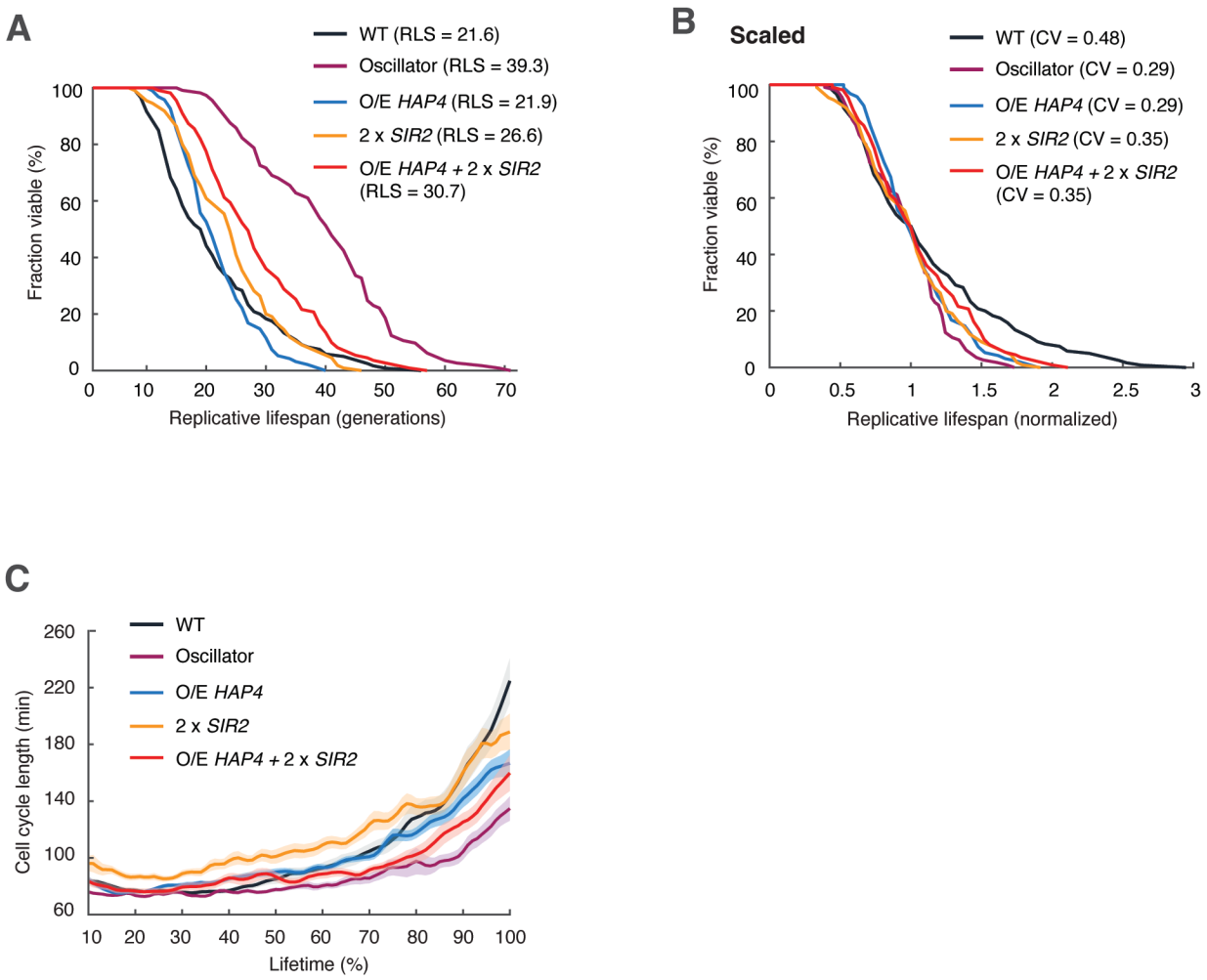

Fig. S11. Comparison of the synthetic oscillator strain with strains constitutively overexpressing *SIR2* and *HAP4*. (A) Replicative lifespans for WT (n=131), the synthetic oscillator strain (n=120), *SIR2* twofold overexpression (2 x *SIR2*, n=92), *HAP4* overexpression (O/E *HAP4*, n=95), and combined *HAP4* overexpression and *SIR2* twofold overexpression (O/E *HAP4* + 2 x *SIR2*, n=97). (B) Lifespan curves for WT, the synthetic oscillator strain, *SIR2* twofold overexpression (2 x *SIR2*), HAP4 overexpression (O/E *HAP4*), and combined *HAP4* overexpression and *SIR2* twofold overexpression (O/E *HAP4* + 2 x *SIR2*), scaled by the median. The Coefficient of Variation (CV) of lifespans among cells was calculated for each strain. (C) Age-dependent changes of cell cycle length for WT, the synthetic oscillator strain, *SIR2* twofold overexpression (2 x *SIR2*), HAP4 overexpression (O/E *HAP4*), and combined *HAP4* overexpression and *SIR2* twofold overexpression (O/E *HAP4* + 2 x *SIR2*).

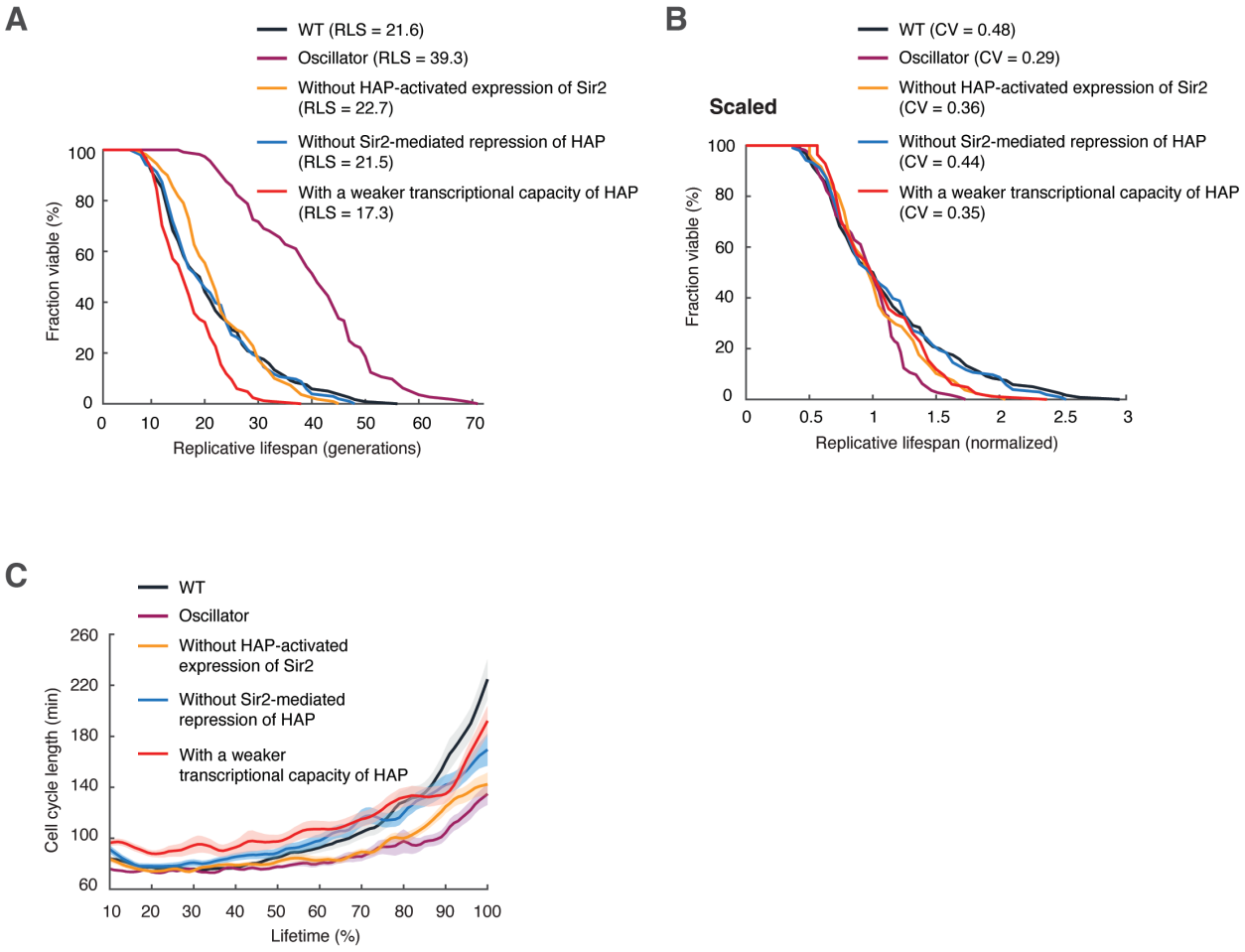

Fig. S12. Comparison of the synthetic oscillator strain with strains carrying synthetic Sir2-HAP circuits with broken or weakened feedback interactions. (A) Replicative lifespans for WT (n=131), the synthetic oscillator strain (n=120), the strain without HAP-activated expression of Sir2 (n=110), the strain without Sir2-mediated repression of HAP (n=103), and the strain with a weaker transcriptional capacity of HAP (n=84). The genetic circuits of these strains are shown in Fig. S9A. (B) Lifespan curves for WT, the synthetic oscillator strain, the strain without HAP-activated expression of Sir2, the strain without Sir2-mediated repression of HAP, and the strain with a weaker transcriptional capacity of HAP, scaled by the median. The Coefficient of Variation (CV) of lifespans among cells was calculated for each strain. (C) Age-dependent changes of cell cycle length for WT, the synthetic oscillator strain, the strain without HAP-activated expression of Sir2, the strain without Sir2-mediated repression of HAP, and the strain with a weaker transcriptional capacity of HAP.

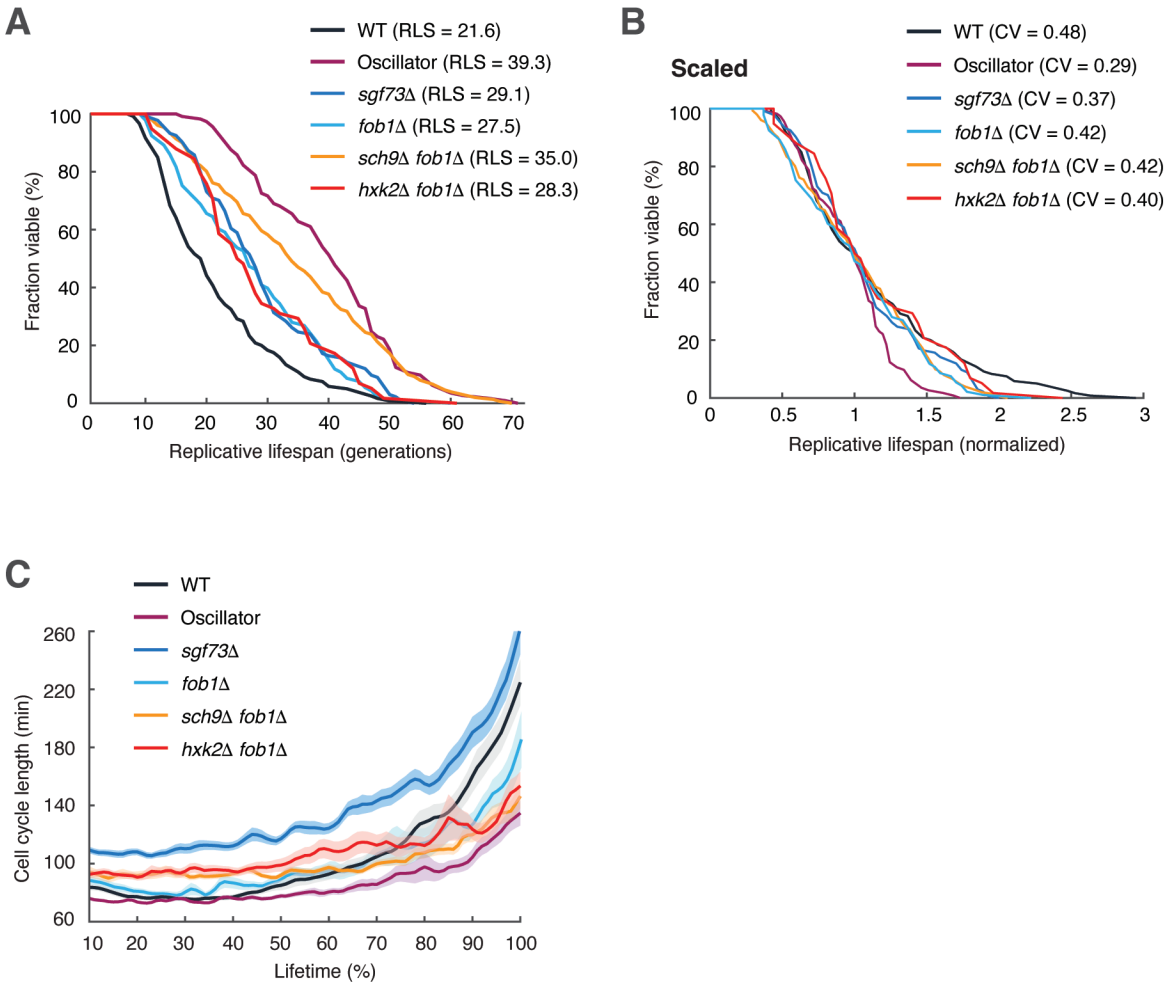

Fig. S13. Comparison of the synthetic oscillator strain with long-lived mutants identified in genetic screens. (A) Replicative lifespans for WT (n=131), the synthetic oscillator strain (n=120), *fob1*Δ (n=93), *sgf73*Δ (n=134), *sch9*Δ *fob1*Δ (n=151), and *hxk2*Δ *fob1*Δ (n=60). The lifespan of the synthetic oscillator strain is significantly longer than that of *sch9*Δ *fob1*Δ ($p = 0.0045$ with Gehan-Breslow-Wilcoxon test). (B) Lifespan curves for WT, the synthetic oscillator strain, *fob1*Δ, *sgf73*Δ, *sch9*Δ *fob1*Δ, and *hxk2*Δ *fob1*Δ, scaled by the median. The Coefficient of Variation (CV) of lifespans among cells was calculated for each strain. (C) Age-dependent changes of cell cycle length for WT, the synthetic oscillator strain, *fob1*Δ, *sgf73*Δ, *sch9*Δ *fob1*Δ, and *hxk2*Δ *fob1*Δ.

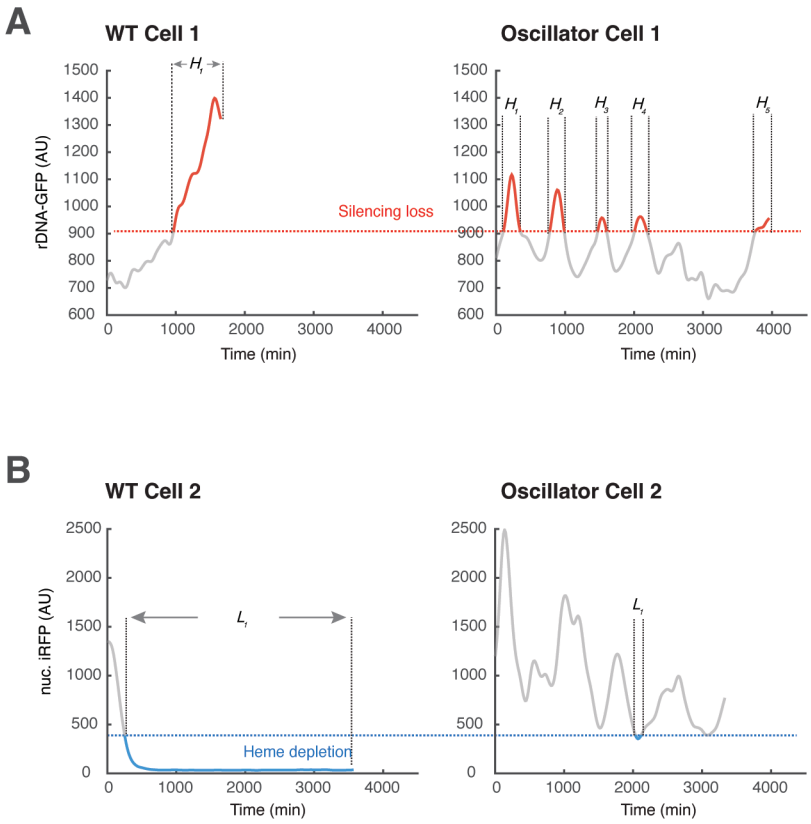

Fig. S14. Quantification of the continuous times at the rDNA silencing loss or heme depletion state. (A) Representative time traces of rDNA-GFP in WT (left) and the synthetic oscillator strain (right) to illustrate the quantification of the continuous times at the rDNA silencing loss state for each single aging cell. The threshold (red dash line) for the state of rDNA silencing loss was defined as the third quartile (75th percentile) of all the rDNA-GFP fluorescence values measured from WT and synthetic oscillator strain. The red portions of time traces above the threshold represent the state of silencing loss. The mean value of the continuous time spans at this state (H_1 for WT and $H_{1\text{-}5}$ for the synthetic oscillator, respectively) was calculated for each single aging cell. (B) Representative time traces of nuc. iRFP in WT (left) and the synthetic oscillator strain (right) to illustrate the quantification of the continuous times at the heme depletion state for each single aging cell. The threshold (blue dash line) for the state of heme depletion was defined as the first quartile (25th percentile) of all the nuc. iRFP fluorescence values measured from the WT and synthetic oscillator strains. The blue portions of time traces below the threshold represent the state of heme depletion. The mean value of the continuous time spans at this state (L_1 for WT and L_1 for the synthetic oscillator) was calculated for each single aging cell. Continuous times at the silencing loss state and the heme depletion state were shown for each single aging cell in Fig. 4C.

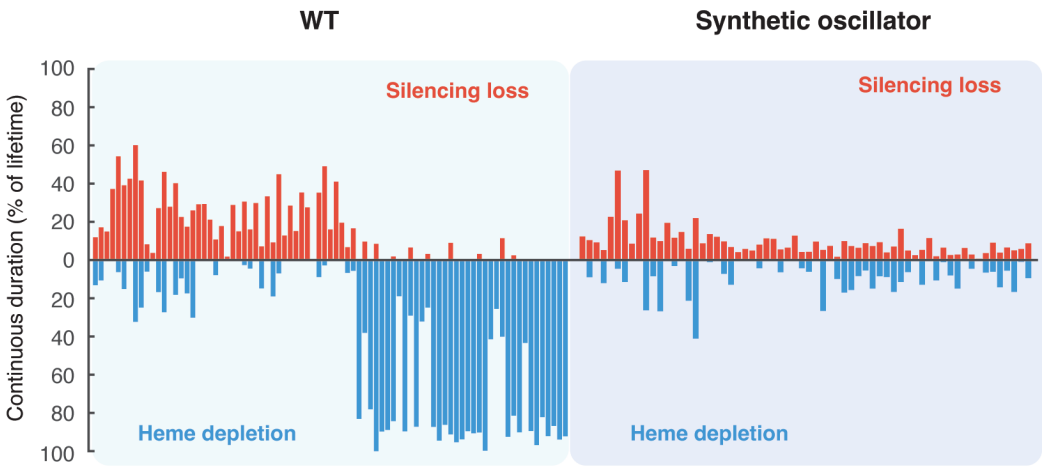

Fig. S15. Bar graphs showing continuous durations (as percentage of the lifetime) of single cells at the rDNA silencing loss or heme depletion state for (left) WT and (right) the synthetic oscillator strain. Each bidirectional bar represents a single cell, in which the red upward portion indicates its continuous duration of the rDNA silencing loss state and the blue downward portion indicates the continuous duration of the heme depletion state, as percentages of its lifetime. The graphs were generated using the data in Fig. 4C. Continuous times for each cell were normalized by its lifetime to facilitate the comparison among strains with different lifetimes.

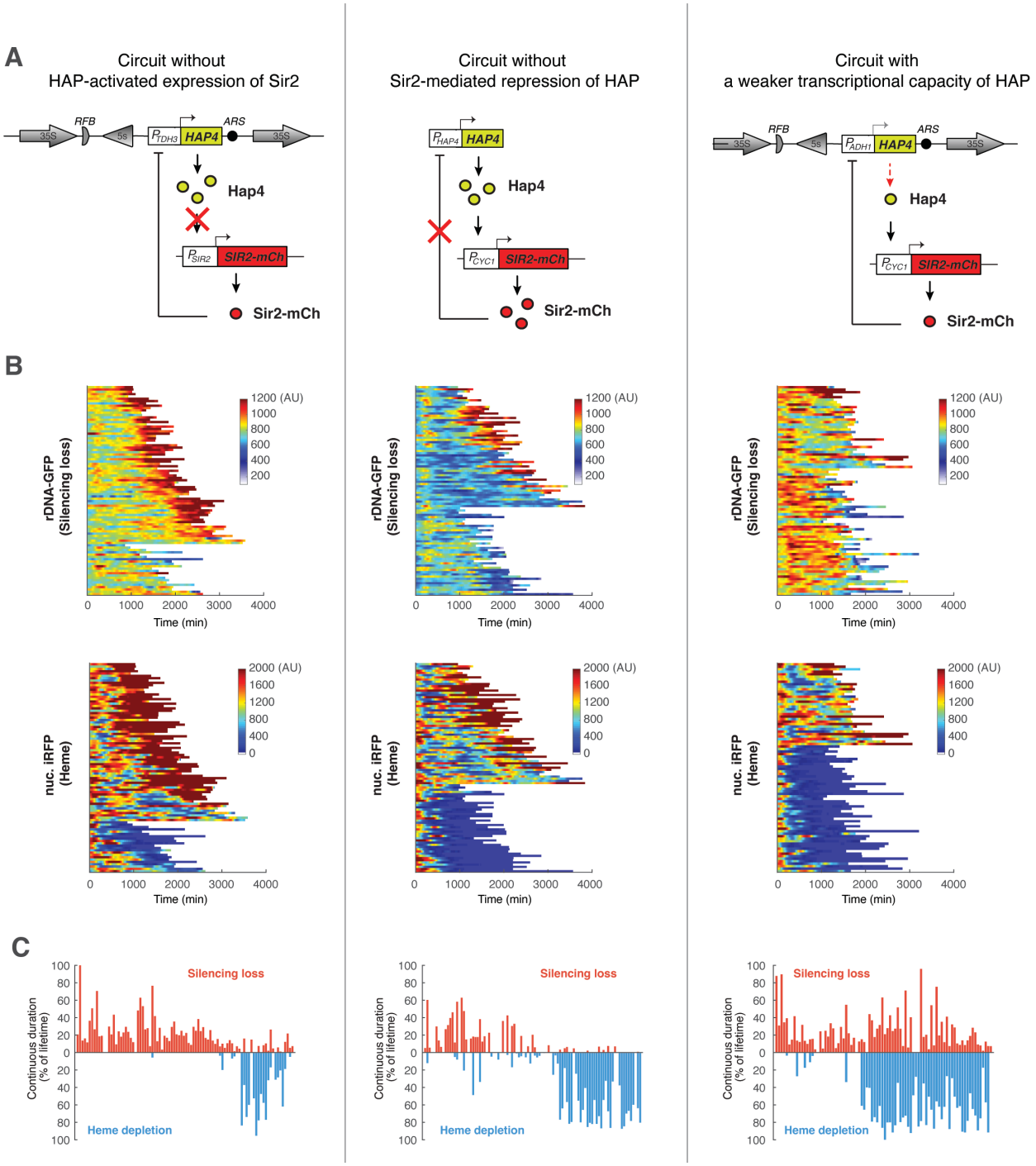

Fig. 16. Synthetic Sir2-HAP circuits with broken or weakened feedback interactions are less able to maintain the balance between rDNA silencing and heme biogenesis. (A) Diagrams illustrate the synthetic Sir2-HAP circuits with broken or weakened interactions. (B) Single-cell color map trajectories of rDNA-GFP (top) and nuclear-anchored iRFP (bottom) in cells carrying the synthetic Sir2-HAP circuits without HAP-activated expression of Sir2 (n=110), without Sir2-mediated repression of HAP (n=103), and with a weaker transcriptional capacity of HAP (n=84). (C) Bar graphs showing continuous durations (as percentage of the lifetime) of single cells at the

rDNA silencing loss or heme depletion state for strains carrying the synthetic Sir2-HAP circuits without HAP-activated expression of Sir2, without Sir2-mediated repression of HAP, and with a weaker transcriptional capacity of HAP.

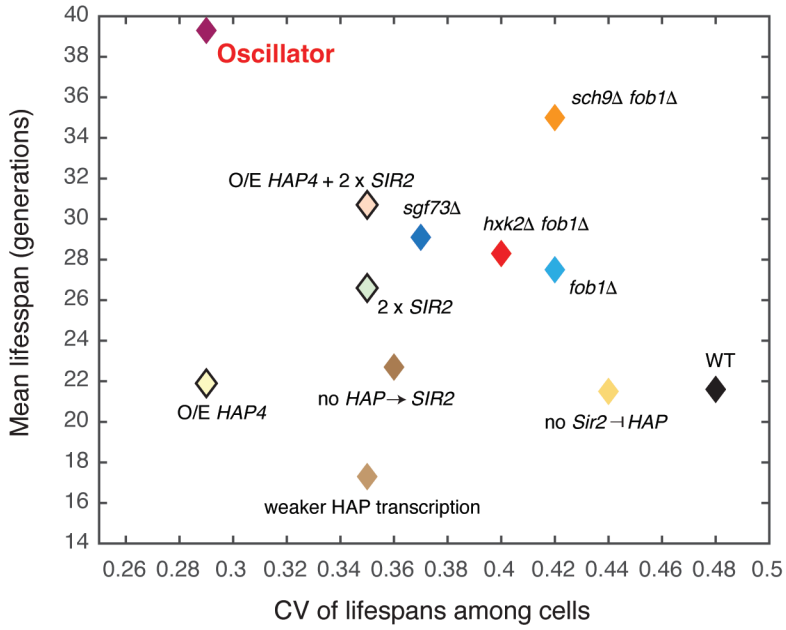

Fig. 17. Scatter plot shows the mean lifespan versus coefficient of variance (CV) of lifespans among cells for all the strains tested in this study. Data are from Figs. S11-13.

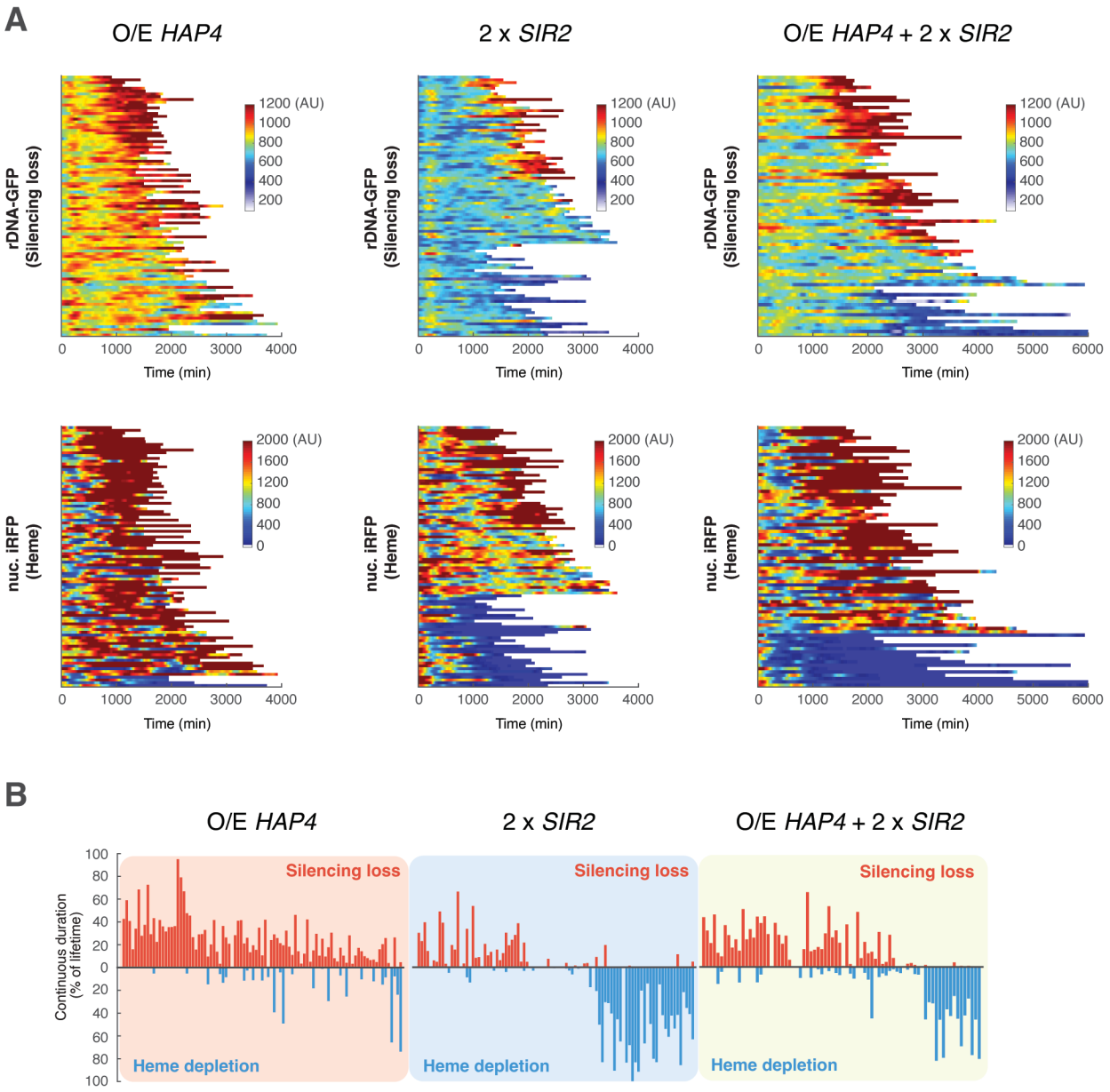

Fig. 18. Strains constitutively overexpressing *SIR2* and *HAP4* are less able to maintain the balance between rDNA silencing and heme biogenesis. (A) Single-cell color map trajectories of rDNA-GFP (top) and nuclear-anchored iRFP (bottom) in cells with *HAP4* overexpression (O/E *HAP4*, n=95), *SIR2* twofold overexpression (2 x *SIR2*, n=92), and combined *HAP4* overexpression and *SIR2* twofold overexpression (O/E *HAP4* + 2 x *SIR2*, n=97). (B) Bar graphs showing continuous durations (as percentage of the lifetime) of single cells at the rDNA silencing loss state or the heme depletion state for O/E *HAP4*, 2 x *SIR2*, and O/E *HAP4* + 2 x *SIR2*.

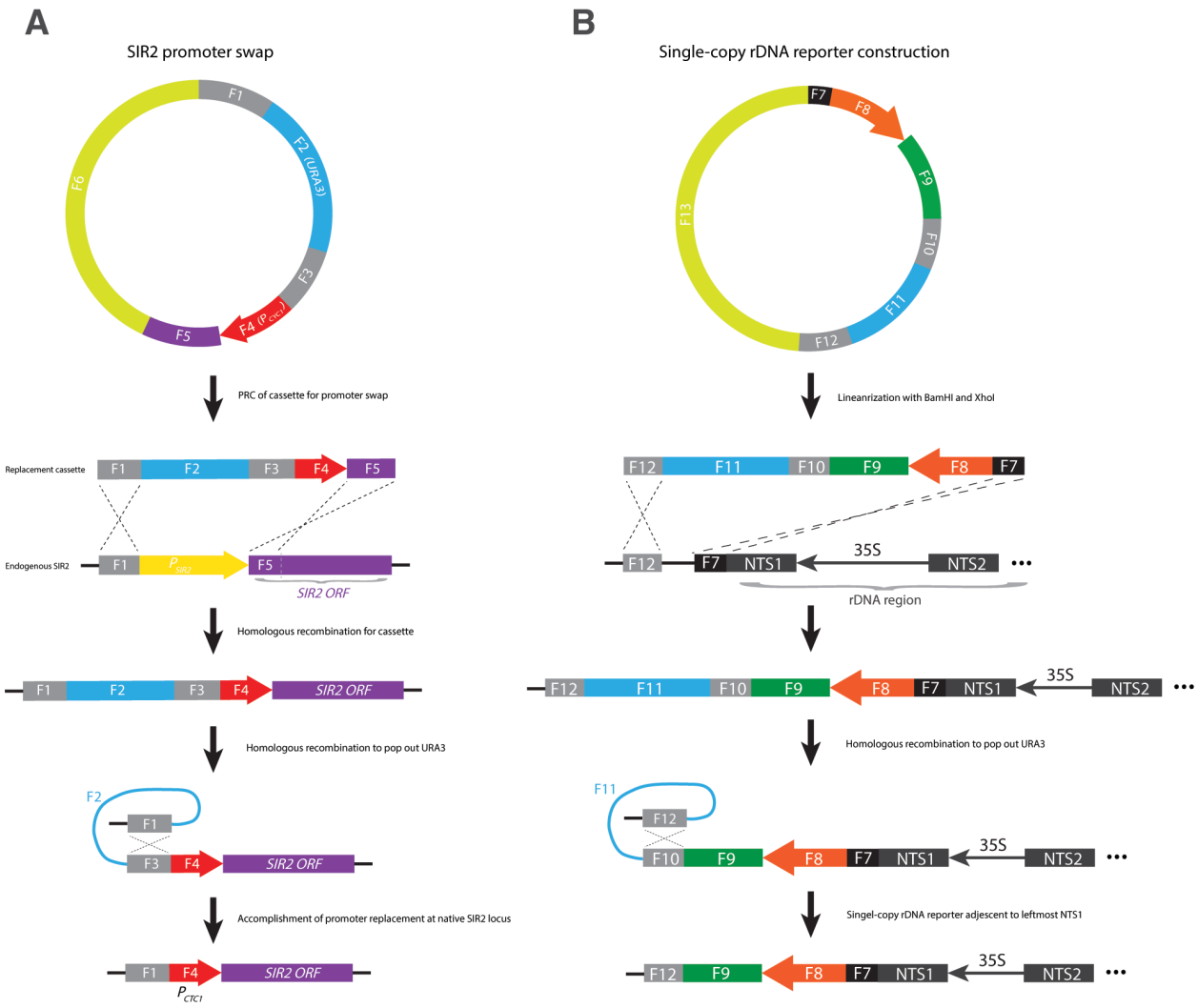

Fig. S19. Illustrations of strain construction. (A) Diagram illustrating the steps for replacing the native *SIR2* promoter by P_{CYC1}. (B) Diagram illustrating the steps for constructing the single-copy rDNA-GFP reporter.

Strain Name	Description
NH0268	*BY4741 MAT*a *his3Δ1 leu2Δ0 met15Δ0 ura3Δ0, NHP6a-iRFP-kanMX*
NH0270	*BY4741 MAT*a *his3Δ1 leu2Δ0 met15Δ0 ura3Δ0, RDN1::NTS1-*P_{TDH3}*-GFP-URA3,NHP6a-iRFP-kanMX*
NH0465	*BY4741 MAT*a *his3Δ1 leu2Δ0 met15Δ0 ura3Δ0, RDN1::NTS1-*P_{TDH3}*-GFP-URA3,NHP6a-iRFP-kanMX, sgf73Δ::HIS3*
NH1378	*BY4741 MAT*a *his3Δ1 leu2Δ0 met15Δ0 ura3Δ0, NHP6a-iRFP-kanMX,* P_{SIR2}*-SIR2-mCherry-LEU2*
NH1382	*BY4741 MAT*a *his3Δ1 leu2Δ0 met15Δ0 ura3Δ0, NHP6a-iRFP-kanMX,* P_{CYC1}*-SIR2-mCherry-LEU2*
NH1391	*BY4741 MAT*a *his3Δ1 leu2Δ0 met15Δ0 ura3Δ0, NHP6a-iRFP-kanMX,* P_{CYC1}*-SIR2-mCherry-LEU2, hap4Δ::HIS3*
NH1545	*BY4741 MAT*a *his3Δ1 leu2Δ0 met15Δ0 ura3Δ0, NHP6a-iRFP-kanMX,* $NTS1_{unique}$*-*P_{TDH3}*-GFP*
NH1571	*BY4741 MAT*a *his3Δ1 leu2Δ0 met15Δ0 ura3Δ0, NHP6a-iRFP-kanMX,* P_{CYC1}*-SIR2-mCherry-LEU2, hap4Δ::HIS3,* $NTS1_{unique}$*-*P_{TDH3}*-GFP*
NH1574	*BY4741 MAT*a *his3Δ1 leu2Δ0 met15Δ0 ura3Δ0, NHP6a-iRFP-kanMX,* P_{CYC1}*-SIR2-mCherry-LEU2, hap4Δ::HIS3,* $NTS1_{unique}$*-*P_{TDH3}*-GFP, RDN1::NTS1-*P_{TDH3}*-HAP4-URA3*
NH1577	*BY4741 MAT*a *his3Δ1 leu2Δ0 met15Δ0 ura3Δ0, NHP6a-iRFP-kanMX,* P_{SIR2}*-SIR2-mCherry-LEU2,* $NTS1_{unique}$*-*P_{TDH3}*-GFP*
NH1701	*BY4741 MAT*a *his3Δ1 leu2Δ0 met15Δ0 ura3Δ0, NHP6a-iRFP-kanMX,* P_{SIR2}*-SIR2-mCherry-LEU2, sch9Δ::HIS3, fob1Δ::URA3*
NH1725	*BY4741 MAT*a *his3Δ1 leu2Δ0 met15Δ0 ura3Δ0, NHP6a-iRFP-kanMX,* $NTS1_{unique}$*-PTDH3-GFP, hap4Δ::LEU2*
NH1802	*BY4741 MAT*a *his3Δ1 leu2Δ0 met15Δ0 ura3Δ0, NHP6a-iRFP-kanMX,* $NTS1_{unique}$*-*P_{TDH3}*-GFP, fob1Δ::LEU2*
NH1808	*BY4741 MAT*a *his3Δ1 leu2Δ0 met15Δ0 ura3Δ0, NHP6a-iRFP-kanMX,* $NTS1_{unique}$*-*P_{TDH3}*-GFP,* P_{TDH3}*-HAP4-HIS3, SIR2::*P_{SIR2}*-SIR2-LEU2*
NH1816	*BY4741 MAT*a *his3Δ1 leu2Δ0 met15Δ0 ura3Δ0, NHP6a-iRFP-kanMX,* $NTS1_{unique}$*-*P_{TDH3}*-GFP, fob1Δ::LEU2, hxk2Δ::URA3*
NH1850	*BY4741 MAT*a *his3Δ1 leu2Δ0 met15Δ0 ura3Δ0, NHP6a-iRFP-kanMX,* P_{SIR2}*-SIR2-mCherry-LEU2,* $NTS1_{unique}$*-*P_{TDH3}*-GFP, RDN1::NTS1-*P_{TDH3}*-HAP4-URA3*
NH1851	*BY4741 MAT*a *his3Δ1 leu2Δ0 met15Δ0 ura3Δ0, NHP6a-iRFP-kanMX,* $NTS1_{unique}$*-*P_{TDH3}*-GFP, hap4Δ::LEU2,* P_{SIR2}*-SIR2-mCherry-HIS3*
NH1852	*BY4741 MAT*a *his3Δ1 leu2Δ0 met15Δ0 ura3Δ0, NHP6a-iRFP-kanMX,* P_{CYC1}*-SIR2-mCherry-LEU2, hap4Δ::HIS3,* $NTS1_{unique}$*-*P_{TDH3}*-GFP; RDN1::NTS1-*P_{ADH1}*-HAP4-URA3*

NH1854	*BY4741 MAT*a *his3Δ1 leu2Δ0 met15Δ0 ura3Δ0, NHP6a-iRFP-kanMX, $NTS1_{unique}$-P_{TDH3}-GFP, hap4Δ::Leu2, P_{SIR2}-SIR2-mCherry-HIS3, RDN1::NTS1-P_{TDH3}-HAP4-URA3*
NH1855	*BY4741 MAT*a *his3Δ1 leu2Δ0 met15Δ0 ura3Δ0, NHP6a-iRFP-kanMX, $NTS1_{unique}$-P_{TDH3}-GFP, SIR2::P_{SIR2}-SIR2-HIS3*
NH1857	*BY4741 MAT*a *his3Δ1 leu2Δ0 met15Δ0 ura3Δ0, NHP6a-iRFP-kanMX, $NTS1_{unique}$-P_{TDH3}-GFP, P_{TDH3}-HAP4-HIS3*

Table S1. Strains used or constructed in this study. All the strains will be available upon request.

Plasmid Name	Description
NHB0299	pRS305--P_{SIR2}-*SIR2*
NHB0638	pRS303-P_{SIR2}-*SIR2*
NHB0659	pRS303-P_{TDH3}-*HAP4*
NHB0730	pZZ-*rDNA-GFP-reporter2.0-URA3* (for single copy rDNA reporter)
NHB1048	pRS306-*NTS1*-P_{TDH3}-*HAP4(HindIII*Δ*)*
NHB1075	pZZ-P_{SIR2}-*T*-P_{CYC1} (for replacing *SIR2* promoter to *CYC1* promoter)
NHB1333	pRS306-*NTS1*-P_{ADH1}-*HAP4(HindIII*Δ*)*

Table S2. Plasmids constructed in this study. All the plasmids will be available upon request.

Primer	Sequence (5'-3')	Description
sir2-tag-F	AGAGAAGGATAAGGGCGTGTATGT CGTTACATCAGATGAACATCCCAA AACCCTCGGTGACGGTGCTGGTTTA	Forward primer for sir2 fluorescence protein tagging, using pKT series plasmid as template
sir2-tag-R	TACTATGTAAATTGATATTAATTTG GCACTTTTAAATTATTAAATTGCCT TCTACTCGATGAATTCGAGCTCG	Reverse primer for sir2 fluorescence protein tagging, using pKT series plasmid as template
hap4del-F	ATTTGTTTTACCTACATTTTCTAGTA CAAAAAAAAAACAAAAAAAGAATC cggcatcagagcagattgtac	Forward primer for HAP4 gene deletion
hap4del-R	TTTGTTTTCGTGATTTTTAGTTGTTT TCGTTTTATTGCAACATGCCTATTgct ttccccgtcaagctctaa	Reverse primer for HAP4 gene deletion
pSir2up@ AmpOri	CCACGCTACTAGTGCCAAGAGTGTT GCTGCTTAT	Forward primer for F1
pSir2up@ Ura3	GCGTGGTGCCTCCAAGGGAGAAAG ACTGC	Reverse primer for F1
Ura3@pSi r2up	CCCTTGGAGGCACCACGCTTTTCAA TTCAA	Forward primer for F2
Ura3@H OMO	GAAGTCCTCCTTAGTTTTGCTGGCC GCATC	Reverse primer for F2
HOMO@ Ura3	CAGCAAAACtaaGGAGGACTTCGCT ACCGA	Forward primer for F3
HOMO@ pCYC1	GTCTCACACGGAAACACATTGAGG AGTTGCAGGCT	Reverse primer for F3
pCYC1@ HOMO	AACTCCTCAATGTGTTTCCGTGTGA GACGACATCG	Forward primer for F4
pCYC1@ Sir2dw	GTGGGATGGTCATTATTAATTTAGT GTGTGTATTTGTG	Reverse primer for F4
Sir2dw@p CYC1	CACTAAATTAATAATGACCATCCCA CATATGAAAT	Forward primer for F5
Sir2dw@ AmpOri	ctcgagATCCTCGGGGAGGTAAGTGT	Reverse primer for F5
AmpOri@ Sir2dw	CTCCCCGAGGATctcgagTATCCGCTC ACAA	Forward primer for F6
AmpOri@ pSir2up	CTTGGCACTAGTAGCGTGGTGCACT CTCAG	Reverse primer for F6
RDNup-pGPD-F	GAAATATCCATTACCCACAGTAAG ACTTTTTTGAATACTCTTTAATATTT TTTatttCAGTTCGAGTTTATCATTATC AATAC	Forward primer for F7-8
pTDH3@ GFP	tcacctttagacatTTTGTTTGTTTATGTGT GTTTATTCG	Reverse primer for F7-8
GFP@pT DH3	ataaacaaacaaaATGTCTAAAGGTGAAG AATTATTCAC	Forward primer for F9

GFP@rdw	AACAATCTTGCGGttatttgtacaattcatccatacc	Reverse primer for F9
rdw@GFP	gaattgtacaaataaCCGCAAGATTGTTCCCAG	Forward primer for F10
rdw@Ura3p	gcctccatgtcATCACCGTTGAGCCTTTTG	Reverse primer for F10
Ura3p@rdw	GCTCAACGGTGATgacatggaggcccagaatac	Forward primer for F11
Ura3@RDNdw	gaacaatcttgcggTTATAATTGGCCAGTCTTTTTCAAATAAG	Reverse primer for F11
rdw@Ura3	aagactggccaattataaCCGCAAGATTGTTCCCAGTAT	Forward primer for F12
rdw@AmpOri	TTTGAGTGAGCTGgatccATCACCGTTGAGCCTTTTG	Reverse primer for F12
XhoAmp-@RDNup	CTTACTGTGGGTAATGGATATTTCtcgAGACGTCAGGTGGCACTTTTC	Forward primer for F13
BamAmp-@RDNdw	ACGGTGATggatcCAGCTCACTCAAAGGC	Reverse primer for F13
Hap4@pRS	gtgggTCAAAATACTTGTACCTTTAAAAAATCG	Forward primer for HAP4 replacing GFP at rDNA silencing reporter
HAP4@pTDH3	CAAACAAAATGACCGCAAAGACTTTTCTAC	Reverse primer for HAP4 replacing GFP at rDNA silencing reporter
pRS@Hap4	AGGTACAAGTATTTTGAcccaccgcggtggagc	Forward primer for PCR out the backbone of rDNA silencing reporter
pTDH3@HAP4	ctttgcggtCATTTTGTTTGTTTATGTGTGTTTATTC	Reverse primer for PCR out the backbone of rDNA silencing reporter
pSIR2-T-F	GCCAAGAGTGTTGCTGCTTAT	Forward primer for PCR out F1-F5
pSIR2-T-R	ATCCTCGGGGAGGTAAGTGTC	Reverse primer for PCR out F1-F5
sir2up-I-F	GTTTGGCGCTGAAAAGATTC	Forward primer for CYC1 promoter replacement checking
pCYC1-I-R	TGCTGCAAAGGTCCTAATGT	Reverse primer for CYC1 promoter replacement checking
GFP-I-F	ttccatggccaaccttagtc	Forward primer for single copy rDNA reporter checking
RDNdw-R	ATCACCGTTGAGCCTTTTGT	Reverse primer for single copy rDNA reporter checking
Hap4-I-F	CTGATTCGCATCACCATGAC	Forward primer for HAP4 gene deletion checking
Hap4-I-R	CGTCGATGAAACTGCTTTGA	Reverse primer for HAP4 gene deletion checking
SIR2ORF-I-F	TGCATCACAGGGTTCAATGT	Forward primer for SIR2 tagging checking

mCherry-I-R	GCA CCG TCT TCT GGG TAC AT	Reverse primer for SIR2 tagging checking
pADH1@Hap4	GTCTTTGCGGTCATTGTATATGAGATAGTTGATTGTATGC	Primer for making NHB1333, use yeast genomic DNA as template
Hap4@pADH1	CAACTATCTCATATACAATGACCGCAAAGACTTTTCTACT	Primer for making NHB1333, use NHB1048 as template
NTS1@pADH1	TGTTCTATTGTATATCTCCggatccCTAGAAACTGCCATTTACTTA	Primer for making NHB1333, use NHB1048 as template
pADH1@NTS1	TTCTAGggatccGGAGATATACAATAGAACAGATACC	Primer for making NHB1333, use yeast genomic DNA as template

Table S3. Primers used in this study.

Parameter	Value	Description
α_S	30.5 h^{-1}	Rate constant of Sir2 transcription
α_H	183 h^{-1}	Rate constant of Hap4 transcription
α_{H0}	0.1 h^{-1}	Rate of Hap4 leaking expression
α_{S0}	0.1 h^{-1}	Rate of Sir2 basal expression
β	3.7 h^{-1}	Rate constant of translation
δ_m	0.3 h^{-1}	Degradation rate of mRNA
δ_H	3.8 h^{-1}	Degradation rate of Hap4
δ_S	0.2 h^{-1}	Degradation rate of Sir2
K_H	326	Median effective concentration for Hap4 activation of *SIR2*
K_S	185	Median effective concentration for Sir2 repression of *HAP4*
n_1	3	Hill coefficient for *SIR2* activation by Hap4
n_2	4.8	Hill coefficient for *HAP4* inhibition by Sir2
τ_H	x h	Time delay for Hap4 effection on *SIR2*; x=0 for four-equations version; x=1 for two-equations version
τ_S	y h	Time delay for Sir2 effection on *HAP4*; y=0 for four-equations version; y=2 for two-equations version

Table S4. Kinetic parameters used in the model.

Movie S1. Time-lapse movie showing oscillations of Sir2-mCherry fluorescence in the synthetic oscillator cell during aging. Right, the movie of a representative engineered cell in which Sir2-mCherry fluorescence were measured during aging. Left, real-time quantification of reporter fluorescence was plotted as a function of time.

References and Notes

1. R. Milo, S. Shen-Orr, S. Itzkovitz, N. Kashtan, D. Chklovskii, U. Alon, Network motifs: Simple building blocks of complex networks. *Science* **298**, 824–827 (2002). doi:10.1126/science.298.5594.824 Medline

2. M. Elowitz, W. A. Lim, Build life to understand it. *Nature* **468**, 889–890 (2010). doi:10.1038/468889a Medline

3. C. J. Bashor, J. J. Collins, Understanding biological regulation through synthetic biology. *Annu. Rev. Biophys.* **47**, 399–423 (2018). doi:10.1146/annurev-biophys-070816-033903 Medline

4. T. S. Gardner, C. R. Cantor, J. J. Collins, Construction of a genetic toggle switch in *Escherichia coli*. *Nature* **403**, 339–342 (2000). doi:10.1038/35002131 Medline

5. M. B. Elowitz, S. Leibler, A synthetic oscillatory network of transcriptional regulators. *Nature* **403**, 335–338 (2000). doi:10.1038/35002125 Medline

6. J. Stricker, S. Cookson, M. R. Bennett, W. H. Mather, L. S. Tsimring, J. Hasty, A fast, robust and tunable synthetic gene oscillator. *Nature* **456**, 516–519 (2008). doi:10.1038/nature07389 Medline

7. A. E. Friedland, T. K. Lu, X. Wang, D. Shi, G. Church, J. J. Collins, Synthetic gene networks that count. *Science* **324**, 1199–1202 (2009). doi:10.1126/science.1172005 Medline

8. T. Danino, O. Mondragón-Palomino, L. Tsimring, J. Hasty, A synchronized quorum of genetic clocks. *Nature* **463**, 326–330 (2010). doi:10.1038/nature08753 Medline

9. A. Becskei, L. Serrano, Engineering stability in gene networks by autoregulation. *Nature* **405**, 590–593 (2000). doi:10.1038/35014651 Medline

10. R. Zhu, J. M. Del Rio-Salgado, J. Garcia-Ojalvo, M. B. Elowitz, Synthetic multistability in mammalian cells. *Science* **375**, eabg9765 (2022). doi:10.1126/science.abg9765 Medline

11. F. Wu, R. Q. Su, Y. C. Lai, X. Wang, Engineering of a synthetic quadrastable gene network to approach Waddington landscape and cell fate determination. *eLife* **6**, e23702 (2017). doi:10.7554/eLife.23702 Medline

12. M. Tigges, T. T. Marquez-Lago, J. Stelling, M. Fussenegger, A tunable synthetic mammalian oscillator. *Nature* **457**, 309–312 (2009). doi:10.1038/nature07616 Medline

13. C. J. Bashor, A. A. Horwitz, S. G. Peisajovich, W. A. Lim, Rewiring cells: Synthetic biology as a tool to interrogate the organizational principles of living systems. *Annu. Rev. Biophys.* **39**, 515–537 (2010). doi:10.1146/annurev.biophys.050708.133652 Medline

14. F. Wu, J. H. Bethke, M. Wang, L. You, Quantitative and synthetic biology approaches to combat bacterial pathogens. *Curr. Opin. Biomed. Eng.* **4**, 116–126 (2017). doi:10.1016/j.cobme.2017.10.007 Medline

15. L. Bintu, J. Yong, Y. E. Antebi, K. McCue, Y. Kazuki, N. Uno, M. Oshimura, M. B. Elowitz, Dynamics of epigenetic regulation at the single-cell level. *Science* **351**, 720–724 (2016). doi:10.1126/science.aab2956 Medline

16. A. J. Keung, C. J. Bashor, S. Kiriakov, J. J. Collins, A. S. Khalil, Using targeted chromatin regulators to engineer combinatorial and spatial transcriptional regulation. *Cell* **158**, 110–120 (2014). doi:10.1016/j.cell.2014.04.047 Medline

17. S. Toda, L. R. Blauch, S. K. Y. Tang, L. Morsut, W. A. Lim, Programming self-organizing multicellular structures with synthetic cell-cell signaling. *Science* **361**, 156–162 (2018). doi:10.1126/science.aat0271 Medline

18. S. Huang, A. J. Lee, R. Tsoi, F. Wu, Y. Zhang, K. W. Leong, L. You, Coupling spatial segregation with synthetic circuits to control bacterial survival. *Mol. Syst. Biol.* **12**, 859 (2016). doi:10.15252/msb.20156567 Medline

19. A. H. Ng, T. H. Nguyen, M. Gómez-Schiavon, G. Dods, R. A. Langan, S. E. Boyken, J. A. Samson, L. M. Waldburger, J. E. Dueber, D. Baker, H. El-Samad, Modular and tunable biological feedback control using a de novo protein switch. *Nature* **572**, 265–269 (2019). doi:10.1038/s41586-019-1425-7 Medline

20. A. V. Belikov, Age-related diseases as vicious cycles. *Ageing Res. Rev.* **49**, 11–26 (2019). doi:10.1016/j.arr.2018.11.002 Medline

21. L. Fontana, L. Partridge, V. D. Longo, Extending healthy life span—From yeast to humans. *Science* **328**, 321–326 (2010). doi:10.1126/science.1172539 Medline

22. V. D. Longo, B. K. Kennedy, Sirtuins in aging and age-related disease. *Cell* **126**, 257–268 (2006). doi:10.1016/j.cell.2006.07.002 Medline

23. B. M. Wasko, M. Kaeberlein, Yeast replicative aging: A paradigm for defining conserved longevity interventions. *FEMS Yeast Res.* **14**, 148–159 (2014). doi:10.1111/1567-1364.12104 Medline

24. M. Kaeberlein, B. K. Kennedy, Large-scale identification in yeast of conserved ageing genes. *Mech. Ageing Dev.* **126**, 17–21 (2005). doi:10.1016/j.mad.2004.09.013 Medline

25. C. He, C. Zhou, B. K. Kennedy, The yeast replicative aging model. *Biochim. Biophys. Acta Mol. Basis Dis.* **1864** (9 Pt A), 2690–2696 (2018). doi:10.1016/j.bbadis.2018.02.023 Medline

26. E. D. Smith, M. Tsuchiya, L. A. Fox, N. Dang, D. Hu, E. O. Kerr, E. D. Johnston, B. N. Tchao, D. N. Pak, K. L. Welton, D. E. L. Promislow, J. H. Thomas, M. Kaeberlein, B. K. Kennedy, Quantitative evidence for conserved longevity pathways between divergent eukaryotic species. *Genome Res.* **18**, 564–570 (2008). doi:10.1101/gr.074724.107 Medline

27. M. R. Gartenberg, J. S. Smith, The nuts and bolts of transcriptionally silent chromatin in *Saccharomyces cerevisiae*. *Genetics* **203**, 1563–1599 (2016). doi:10.1534/genetics.112.145243 Medline

28. M. Kaeberlein, M. McVey, L. Guarente, The *SIR2/3/4* complex and *SIR2* alone promote longevity in *Saccharomyces cerevisiae* by two different mechanisms. *Genes Dev.* **13**, 2570–2580 (1999). doi:10.1101/gad.13.19.2570 Medline

29. K. Saka, S. Ide, A. R. Ganley, T. Kobayashi, Cellular senescence in yeast is regulated by rDNA noncoding transcription. *Curr. Biol.* **23**, 1794–1798 (2013). doi:10.1016/j.cub.2013.07.048 Medline

30. D. A. Sinclair, L. Guarente, Extrachromosomal rDNA circles—A cause of aging in yeast. *Cell* **91**, 1033–1042 (1997). doi:10.1016/S0092-8674(00)80493-6 Medline

31. S. Buschlen, J.-M. Amillet, B. Guiard, A. Fournier, C. Marcireau, M. Bolotin-Fukuhara, The *S. Cerevisiae* HAP complex, a key regulator of mitochondrial function, coordinates nuclear and mitochondrial gene expression. *Comp. Funct. Genomics* **4**, 37–46 (2003). doi:10.1002/cfg.254 Medline

32. Y. Li, M. Jin, R. O'Laughlin, P. Bittihn, L. S. Tsimring, L. Pillus, J. Hasty, N. Hao, Multigenerational silencing dynamics control cell aging. *Proc. Natl. Acad. Sci. U.S.A.* **114**, 11253–11258 (2017). doi:10.1073/pnas.1703379114 Medline

33. G. S. Filonov, K. D. Piatkevich, L.-M. Ting, J. Zhang, K. Kim, V. V. Verkhusha, Bright and stable near-infrared fluorescent protein for in vivo imaging. *Nat. Biotechnol.* **29**, 757–761 (2011). doi:10.1038/nbt.1918 Medline

34. Y. Li, Y. Jiang, J. Paxman, R. O'Laughlin, S. Klepin, Y. Zhu, L. Pillus, L. S. Tsimring, J. Hasty, N. Hao, A programmable fate decision landscape underlies single-cell aging in yeast. *Science* **369**, 325–329 (2020). doi:10.1126/science.aax9552 Medline

35. J. Olesen, S. Hahn, L. Guarente, Yeast *HAP2* and *HAP3* activators both bind to the *CYC1* upstream activation site, UAS2, in an interdependent manner. *Cell* **51**, 953–961 (1987). doi:10.1016/0092-8674(87)90582-4 Medline

36. L. Guarente, T. Mason, Heme regulates transcription of the *CYC1* gene of *S. cerevisiae* via an upstream activation site. *Cell* **32**, 1279–1286 (1983). doi:10.1016/0092-8674(83)90309-4 Medline

37. S. Hahn, L. Guarente, Yeast *HAP2* and *HAP3*: Transcriptional activators in a heteromeric complex. *Science* **240**, 317–321 (1988). doi:10.1126/science.2832951 Medline

38. C. Li, J. E. Mueller, M. Bryk, Sir2 represses endogenous polymerase II transcription units in the ribosomal DNA nontranscribed spacer. *Mol. Biol. Cell* **17**, 3848–3859 (2006). doi:10.1091/mbc.e06-03-0205 Medline

39. C. M. Gallo, D. L. Smith Jr., J. S. Smith, Nicotinamide clearance by Pnc1 directly regulates Sir2-mediated silencing and longevity. *Mol. Cell. Biol.* **24**, 1301–1312 (2004). doi:10.1128/MCB.24.3.1301-1312.2004 Medline

40. B. Ho, A. Baryshnikova, G. W. Brown, Unification of protein abundance datasets yields a quantitative *Saccharomyces cerevisiae* proteome. *Cell Syst.* **6**, 192–205.e3 (2018). doi:10.1016/j.cels.2017.12.004 Medline

41. L. Xiong, Y. Zeng, R.-Q. Tang, H. S. Alper, F.-W. Bai, X.-Q. Zhao, Condition-specific promoter activities in *Saccharomyces cerevisiae*. *Microb. Cell Fact.* **17**, 58 (2018). doi:10.1186/s12934-018-0899-6 Medline

42. W. Dang, K. K. Steffen, R. Perry, J. A. Dorsey, F. B. Johnson, A. Shilatifard, M. Kaeberlein, B. K. Kennedy, S. L. Berger, Histone H4 lysine 16 acetylation regulates cellular lifespan. *Nature* **459**, 802–807 (2009). doi:10.1038/nature08085 Medline

43. T. Smeal, J. Claus, B. Kennedy, F. Cole, L. Guarente, Loss of transcriptional silencing causes sterility in old mother cells of *S. cerevisiae*. *Cell* **84**, 633–642 (1996). doi:10.1016/S0092-8674(00)81038-7 Medline

44. M. A. McCormick, A. G. Mason, S. J. Guyenet, W. Dang, R. M. Garza, M. K. Ting, R. M. Moller, S. L. Berger, M. Kaeberlein, L. Pillus, A. R. La Spada, B. K. Kennedy, The SAGA histone deubiquitinase module controls yeast replicative lifespan via Sir2 interaction. *Cell Rep.* **8**, 477–486 (2014). doi:10.1016/j.celrep.2014.06.037 Medline

45. M. Kaeberlein, K. T. Kirkland, S. Fields, B. K. Kennedy, Sir2-independent life span extension by calorie restriction in yeast. *PLOS Biol.* **2**, e296 (2004). doi:10.1371/journal.pbio.0020296 Medline

46. M. Kaeberlein, R. W. Powers 3rd, K. K. Steffen, E. A. Westman, D. Hu, N. Dang, E. O. Kerr, K. T. Kirkland, S. Fields, B. K. Kennedy, Regulation of yeast replicative life span by TOR and Sch9 in response to nutrients. *Science* **310**, 1193–1196 (2005). doi:10.1126/science.1115535 Medline

47. M. Jin, Y. Li, R. O'Laughlin, P. Bittihn, L. Pillus, L. S. Tsimring, J. Hasty, N. Hao, Divergent aging of isogenic yeast cells revealed through single-cell phenotypic dynamics. *Cell Syst.* **8**, 242–253.e3 (2019). doi:10.1016/j.cels.2019.02.002 Medline

48. L. Guarente, C. Kenyon, Genetic pathways that regulate ageing in model organisms. *Nature* **408**, 255–262 (2000). doi:10.1038/35041700 Medline

49. M. Kuningas, S. P. Mooijaart, D. van Heemst, B. J. Zwaan, P. E. Slagboom, R. G. J. Westendorp, Genes encoding longevity: From model organisms to humans. *Aging Cell* **7**, 270–280 (2008). doi:10.1111/j.1474-9726.2008.00366.x Medline

50. M. A. McCormick, J. R. Delaney, M. Tsuchiya, S. Tsuchiyama, A. Shemorry, S. Sim, A. C.-Z. Chou, U. Ahmed, D. Carr, C. J. Murakami, J. Schleit, G. L. Sutphin, B. M. Wasko, C. F. Bennett, A. M. Wang, B. Olsen, R. P. Beyer, T. K. Bammler, D. Prunkard, S. C. Johnson, J. K. Pennypacker, E. An, A. Anies, A. S. Castanza, E. Choi, N. Dang, S. Enerio, M. Fletcher, L. Fox, S. Goswami, S. A. Higgins, M. A. Holmberg, D. Hu, J. Hui, M. Jelic, K.-S. Jeong, E. Johnston, E. O. Kerr, J. Kim, D. Kim, K. Kirkland, S. Klum, S. Kotireddy, E. Liao, M. Lim, M. S. Lin, W. C. Lo, D. Lockshon, H. A. Miller, R. M. Moller, B. Muller, J. Oakes, D. N. Pak, Z. J. Peng, K. M. Pham, T. G. Pollard, P. Pradeep, D. Pruett, D. Rai, B. Robison, A. A. Rodriguez, B. Ros, M. Sage, M. K. Singh, E. D. Smith, K. Snead, A. Solanky, B. L. Spector, K. K. Steffen, B. N. Tchao, M. K. Ting, H. Vander Wende, D. Wang, K. L. Welton, E. A. Westman, R. B. Brem, X. G. Liu, Y. Suh, Z. Zhou, M. Kaeberlein, B. K. Kennedy, A comprehensive analysis of replicative lifespan in 4,698 single-gene deletion strains uncovers conserved mechanisms of aging. *Cell Metab.* **22**, 895–906 (2015). doi:10.1016/j.cmet.2015.09.008 Medline

51. Z. Zhou, zhoutopo/science_aging_model: science, Zenodo (2021); https://doi.org/10.5281/zenodo.7407339.

52. S. W. Buck, J. J. Sandmeier, J. S. Smith, RNA polymerase I propagates unidirectional spreading of rDNA silent chromatin. *Cell* **111**, 1003–1014 (2002). doi:10.1016/S0092-8674(02)01193-5 Medline

53. Ž. Pušnik, M. Mraz, N. Zimic, M. Moškon, Computational analysis of viable parameter regions in models of synthetic biological systems. *J. Biol. Eng.* **13**, 75 (2019). doi:10.1186/s13036-019-0205-0 Medline

54. A. Dhooge, W. Govaerts, Y. A. Kuznetsov, H. G. E. Meijer, B. Sautois, New features of the software MatCont for bifurcation analysis of dynamical systems. *Math. Comput. Model. Dyn. Syst.* **14**, 147–175 (2008). doi:10.1080/13873950701742754

55. J. Paxman, Z. Zhou, R. O'Laughlin, Y. Liu, Y. Li, W. Tian, H. Su, Y. Jiang, S. E. Holness, E. Stasiowski, L. S. Tsimring, L. Pillus, J. Hasty, N. Hao, Age-dependent aggregation of ribosomal RNA-binding proteins links deterioration in chromatin stability with challenges to proteostasis. *eLife* **11**, e75978 (2022). doi:10.7554/eLife.75978 Medline

56. R. O'Laughlin, M. Jin, Y. Li, L. Pillus, L. S. Tsimring, J. Hasty, N. Hao, Advances in quantitative biology methods for studying replicative aging in *Saccharomyces cerevisiae*. *Transl. Med. Aging* **4**, 151–160 (2020). doi:10.1016/j.tma.2019.09.002 Medline

57. M. Lavielle, Using penalized contrasts for the change-point problem. *Signal Processing* **85**, 1501–1510 (2005). doi:10.1016/j.sigpro.2005.01.012

58. R. Killick, P. Fearnhead, I. A. Eckley, Optimal detection of changepoints with a linear computational cost. *J. Am. Stat. Assoc.* **107**, 1590–1598 (2012). doi:10.1080/01621459.2012.737745